TEMPERATURE DEPENDENCE OF THE OPTICAL PROPERTIES OF a-Si:H THIN FILMS FOR SOLAR CELLS

A THESIS SUBMITTED TO
THE SCHOOL OF GRADUATE STUDIES
ADDIS ABABA UNIVERSITY

IN PARTIAL FULFILLMENT OF THE
REQUIREMENTS FOR THE DEGREE OF
MASTER OF SCIENCE IN PHYSICS

BY

CHALLA BEKELE
ADDIS ABABA, ETHIOPIA
JUNE, 1996

CONTENTS

ACKNOWLEDGEMENTS

I would like to express my heart felt gratitude to Dr . Fisseha Kasahun for he has helped me to join graduate study programme in physics. I am also very grateful to my friend Endeshaw Hailu for his consistent encouragement and support throughout the study programme.

I would also like to express my heart felt gratitude to Prof. Dr . H . Wagner for he allowed me to join solar cell characterization research group at Institute of Thin Film and Ion Technology (ISI - PV) KFA - Juelich ,Germany where this work was done.

I am also greatly indepted to my Advisor Dr . Th . Eickhoff for accepting me in his research group , consistent advise , guidance and invaluable suggestions throughout the work .

My special thanks go to Ms. K . Winz for her practical assistance and unreserved help in facilitating the work . My best gratitude also goes to Mr . F . Birmans for preparation of the cryostat holder at the workshop and also ISI - PV work shop particularly Mr . Schwan for timely response to preparation of other accessories required for the work.

I extend my warmest gratitude to all members of ISI - PV group for their unreserved assistance, conducive working atmosphere during my stay there.

It is my pleasure to thank my Advisor in Ethiopia Dr . Ulrich Stutenbaeumer for his valuable comments and suggestions.

Last but not least, I would like to thank DAAD (Deutscher Akademischer Austauschdienst) for financing my thesis work.

ABSTRACT

In the fundamental absorption region, near normal incidence reflectance R and transmittance T measurements can provide information about optical properties of thin films [1] . Temperature dependent optical properties of p - , i - , n - layers of a-Si:H films have been studied. The behavior of reflectance R and transmittance T as a function of temperature of a-Si:H thin films is analyzed. From temperature dependence of R and T the temperature dependence of the absorption coefficent (α) is calculated using Hishikawa relation. From the temperature dependent absorption coefficient, the variation of the optical energy gap of the films with temperature is determined. Finally its effect on solar cell applications is discussed.

INTRODUCTION

World wide, the energy supply is continuously dependent on energy sources whose material is very limited. In addition they cause risk for the environment and climate; greenhouse - effect in case of fossils, and radiation risk in case of nuclear energy. Therefore, research is being carried out on the one hand to use energy more efficiently and economically and on the other hand to replace fossil and nuclear energy sources by other means : Here the chance is opened for renewable energy, which also gives an interesting perspective for 3rd world countries.

One of the regenerative energy sources is the direct transformation of solar energy into electric energy - Photovoltaics. Conceptually, in its simplest form a photovoltaic device is a solar - powered battery whose only consumable is the light that fuels it [2] . It is environmentally friendly and particularily interesting as a dis-centeralized energy source. Because sunlight is universally available, it is usable and acceptable to all inhibitants of our planet .

The research goal in this area is to make the transformation more effective and to reduce the cost of production of the solar cells. Solar cell from hydrogenated amorphous Silicon (a-Si:H) is of advantage in material consumption and large area production cost in comparison to solar cells from crystalline or polycrystalline silicon. However, the efficiency of a-Si:H solar cells is lower and its long-time-stability worse .Therefore, currently there is intensive research going on in order to improve such behavior of a-Si:H solar cells.

In addition to low efficiency in a-Si:H cells, it was proved that the operating temperature has significant effect on its efficiency. Short circuit currents and open - circuit voltages are directly related to the optical absorption coefficients and optical band gaps [3], respectively, which are themselves dependent on temperature. It was also reported [4] that with decreasing temperature, both the blue and red response of an a-Si:H p-i-n solar cells decrease. Thus, it is important to investigate the effect of operating temperature on a-Si:H solar cells quantitatively.

A precise determination of the temperature dependence of the optical constants of all layers and their inclusion into the multilayer optical behavior of the solar cell is the primary motive of this work. With increase in temperature the energy gap decreases; also the absorption coefficient $\alpha(E)$ was found to increase for arbitrary but fixed energy. This would lead to the increase of spatially dependent generation rate G(x,E). Therefore, from this result one would expect that J_{ph} increases with increasing temperature. This is valid provided that the charge carrier collection via field plus recombination is not drastically affected with temperature. However, it is indeed altered - in particular under blue light illumination[4].

In this work, section two introduces solar cell operation principles. In section three the optical constants of thin - films is defined and the general properties of the film such as optical gap, densities of states (DOS), defects and hydrogenation effects and the absorption processes was considered. In section four the temperature dependence of the energy gap in semiconductors is discussed.

In section five the experimental details is given; and in sections six and seven the experimental results, discussions and conclusions was presented respectively. In the last section references was given .

2. P-I-N Solar cell Operation

In this section the operation principle of amorpous Silicon P-I-N solar cells are introduced and discussed.

2 . 1 Light Absorption

The first step of the photovoltaic energy conversion in the semiconductor based solar cells is the optical absorption of photons in the semiconductor material, leading to the creation of free electron-hole pairs. This absorption can be regarded independently of the subsequent steps of separation and collection of the resulting electrical carriers in the semiconductor junction.

Figure 2.1 shows the optical absorption of hydrogenated amorphous Silicon (a-Si:H) as a function of the wavelength of the light. Additionally, the absorption of the crystalline and the AM 1.5 solar spectrum power density are plotted. The most relevant feature of the absorption curve of a-Si:H is a greater absorption in the wavelength region from 300 - 700 nm compared to that of crystalline Silicon. It is this high optical absorption that makes amorphous Silicon a suitable thin - film for solar cell material. The horizontal line in Figure 2.1 give an estimate of the absorption limit of films with different thicknesses.

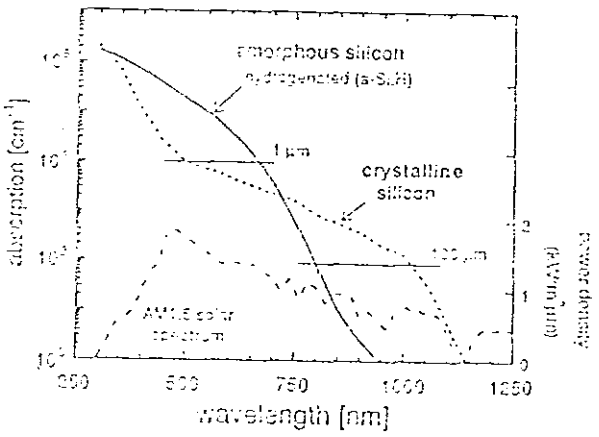

Fig . 2.1 optical absorption coefficient of a - Si:H and c-Si and AM 1.5 million2 [5].

At a thickness of 1μm, an a-Si:H can absorb the light up to a wavelength much longer than a c-Si film of the same thickness. The sharp decrease of the absorption of a-Si:H at higher wavelengths on the other hand makes it virtually impossible to exploit the fraction of the sun spectrum above 750 nm with a-Si:H (by alloying a-Si:H with Germanium (a-$Si_x Ge_{1-x}$), the absorption can be extended to about 900 nm .

Figure 2.2 shows the carrier generation rate G(x) [6,12] in a-Si:H, as the function of the penetration depth x, as produced by the AM 1.5 solar spectrum (at 1000W/m^2) .

$$G(x) = \int_0^\infty P_{AM1.5}(\lambda)\frac{\lambda}{hc}\alpha(\lambda)e^{-x\alpha(\lambda)}d\lambda$$

and the resulting cummulative photogeneration current [6] $J_{Light}(L)$

$$J_{light}(L) = e\int_0^L G(x)dx$$

where P is the spectral power, α is the absorption coefficient and e is the elementary charge.

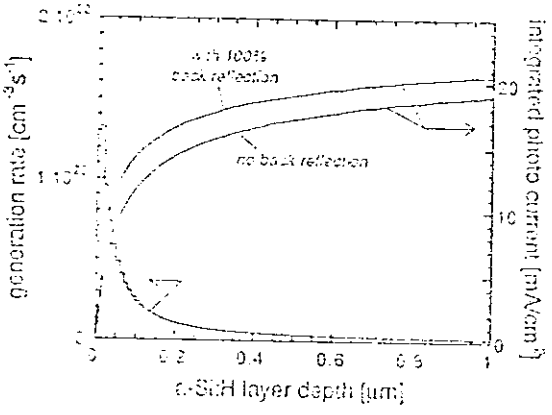

Figure 2.2 Calculated generation rate as a function of penetration depth, and totally generated photon current to this depth for single and double light pass , in a-Si:H layer(same absorption coefficent as in figure 2.1 and same solar spectrum) [5].

The generation rate sharply decays in the first few tenths of a micrometer, and for thickness greater than 0.5 μm the resulting photocurrent saturates towards a value of about 20 mA/cm^2 . In practice, two effects lead to deviation from the theoretical curve. First different loss mechanisms reduce the usable photocurrent. The losses include reflection and transmission losses in non-photovoltaically active overlayers, e.t.c. On the other hand, various "optical enhancement" schemes can increase the photocurrent by lengthening the optical path of the light . For example the absorption probability is increased by reflection at the back side of the layer (if the reflection is 100%, the thickness required to absorb a given photocurrent is reduced to one half, as indicated in figure 2.2, and by other than perpendicular angle of incidence of the light as realized by using textured substrates such as Transparent Conductive Oxides (TCO).

2.2 Carrier Collection in P-I-N Solar Cells

To produce electrical power available on external electric terminals, i.e to realize photovoltaic energy conversion , the photogenerated electrons and holes have to be separated in suitable electronic devices. It is thereby crucial to prevent the recombination of the electrons and holes in the absorbing material itself. Typically, the separation is achieved by electrostatic barriers that are induced in solar cell through an appropriate doping scheme.

Due to the high recombination probability in amorphous Silicon, p-i-n diodes have proven to be the most succesful solar cell design for a-Si:H. In a p-i-n device, the electrostatic barrier between a p-doped and a n-doped layer (the built in potential V_{bi}) is used to induce an electric field into a non-doped, intrinsic layer (i-layer), which extends over most of the solar cell (figure 2.3). In this intrinsic layer, the electric field enhances the carrier transport to a degree that allows for the collection of the photocarriers before they recombine. In the highly doped p- and n-layers of the a-Si:H p-i-n solar cells virtually all the photocarriers are lost because of an even increased recombination as compared to intrinsic a-Si:H material [7], i.e., these layers are "photovoltically dead". The thickness of the doped layers is therefore reduced to the minimum needed to form the barrier; this thickness is of the order of 10-20 nm .

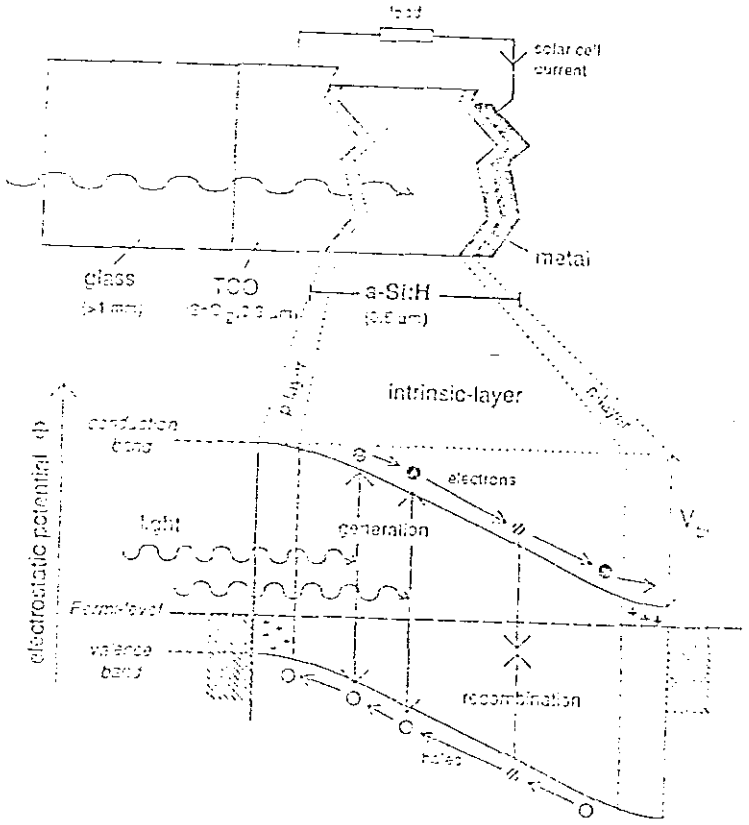

Figure 2.3 : schematic physical structure (top), and band - diagram and photocarrier collection (bottom) in a - Si : H p - i - n solar cell [5] .

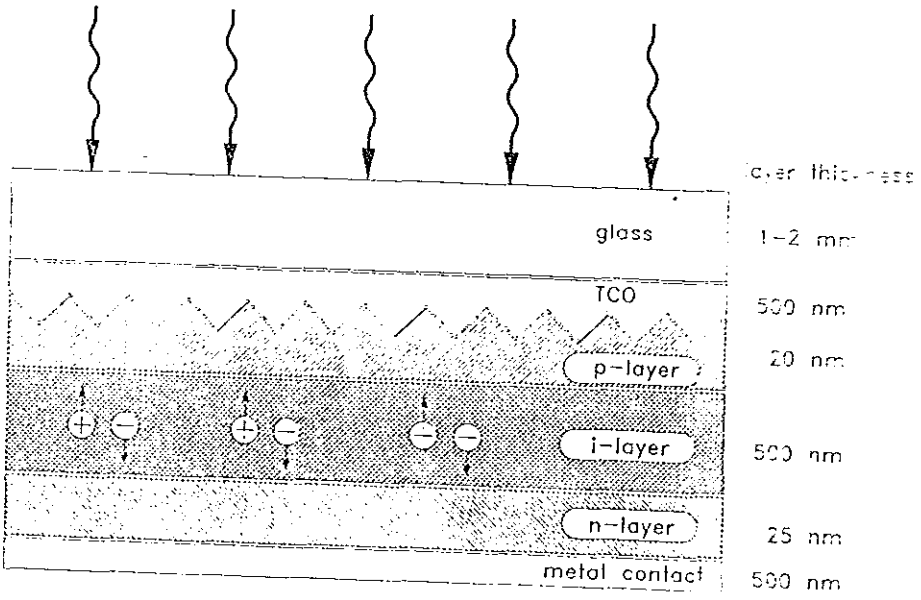

Figure 2.4 Typical p - i - n a -Si:H solar cell structure [3].

3 Optical Constants

3.1 Definitions [9] :

Let us consider the effect of a monochromatic plane wave of angular frequency ω and wave vector q traveling through an absorbing medium. The electromagnetic radiation incident on a medium causes an electric polarization by the induced dipole moments of the molecules (a permanent dipole moment is here excluded). As the perturbing effect of the electromagneric wave is usually very small, the relation between the macroscopic electric field E and the electric polarization P is linear:

$$D = E + 4\pi P = \varepsilon E$$

The complex dielectric constant ε represents the response of the medium to the electromagnetic radiation. If N is the complex refractive index, then

$$\varepsilon = \varepsilon_1 + i\varepsilon_2 = N^2 = (n^2 - \eta^2) + 2in\eta$$

where n is the index of refraction and η the extinction coefficient . The electromagnetic field in absorbing medium can be represented by the relation :

$$E(r,t) = E_0 \exp i(q.r - \omega t) \qquad (2.1)$$

$$H(r,t) = H_0 \exp i(q.r - \omega t) \qquad (2.2)$$

where q is the complex propagation vector; $q = q_1 + i\, q_2$ and the imaginary part governs the attenuation of the wave. Equations (2.1) and (2.2) form the solution of Maxwell's equation[36] for uncharged medium of magnetic permeability $\mu = 1$, if

$$q.q = \varepsilon\omega^2/c^2 \qquad (2.3)$$

If q_1 and q_2 are parallel (homogeneous plane wave), the two fields and directions of propagation are mutually perpendicular and we find from equations (2.3)

$$q_1 = n\omega/c \quad \text{and} \quad q_2 = \eta\omega/c$$

In this case the time averaged energy flow is given by

$$s = \frac{1}{2} nc\varepsilon_0 (E^* . E) e_q$$

where e_q is a unit vector in the direction of q. With the expression for E from equation (2.1) :

$$s = \frac{1}{2} nc\varepsilon_0 (E_0^* . E_0) e_q \exp(-2q_2 r) .$$

It is seen that the energy flow decreases by a factor $exp(-2q_2 d)$ over the distance d. The absorption coefficient α, defined by the relative decrease of energy flow per unit distance in the direction of propagation (λ being wavelength in vacuum), is thus :

$$\alpha = 2q_2 = 2\eta\omega/c = 4\pi\eta/\lambda$$

3.2 Optical Gap

The dielectric function $\varepsilon_2(\omega)$ for a crystalline semiconductor is given by [10,11]

$$\varepsilon_2(\omega) = \left(\frac{2\pi e}{m\omega}\right) \frac{2}{(2\pi)^3} \int_{Bz} d^3k \, |p_{cv}(k)|^2 \quad \delta[E_c(k) - E_v(k) - \hbar\omega] \qquad (3.1)$$

where P_{cv} (k) is the momentum matrix element, c and v denote the conduction and valence bands, respectively, E_c (k) -E_v (k) is the interband energy, and the integration is performed over the first *BZ*.

It is well known that the valence and conduction bands retain their meaning even in amorphous state. Assuming the basic volume V contains the same number of atoms in

amorphous as in the crystalline state and that $P_{cv}(k)$ is independent of wave vector one obtain [13]

$$\varepsilon_2(\omega) = (\frac{2\pi e}{m\omega})\frac{(2\pi)^3}{2B_0}P_{cv}^2\int g_c(E^*)g_v(\hbar\omega - E^*)dE^* \qquad (3.2)$$

where g_c and g_v are the densities of states in the conduction and valence bands, respectively . It is apparent that $\varepsilon_2(\omega)$ is determined by the convolution of densities of states in the conduction and valence bands g_c and g_v for which energy is conserved. If for example the density of states at the bottom of the conduction band is represented by $g_c \propto (E - E_c)^S$ and at the top of the valence band by $g_v \propto (E_v - E)^P$ and if the band edges are parabolic ($p = s = 1/2$) then [9]:

$$\varepsilon_2(\omega) = D(\hbar\omega)^{-2}(\hbar\omega - E_g)^2 \qquad (3.3)$$

where D is a nondimensional strength parameter and E_g is the optical energy gap. If the transition involves band tails which are assumed to be linear in energy, i.e., if $s = p = 1$, then $\varepsilon_2 \alpha (\hbar\omega - E_g)^3$. The fundamental absorption corresponds to band - to - band transition and manifests itself by a rapid rise in absorption. In the energy range where fundamental absorption occurs the experimental $\varepsilon_2(\omega)$ follows the relation above. Such behavior is observed for amorphous semiconductors and insulators. If we plot $\hbar\omega[\varepsilon_2(\omega)]^{1/2}$ versus $\hbar\omega$ (Tauc plot [15]) near the band gap, then we get the values of D and E_g from the linear extrapolation of the plot . Neglecting exciton formation $\alpha(h\nu)$ depends on the joint density of states for bands containing the initial and final states. For simple parabolic bands $g(E) \propto E^{1/2}$, for direct transitions (amorphous semiconductors), the absorption is given by (D and B are related by $D = \hbar ncB$)

$$\alpha\hbar\omega = B(\hbar\omega - E_g)^m \qquad (3.4)$$

for constant index of refraction and m = 2 or 3 depending on parabolic or linear band edge respectively. The most important features of optical absorption processes in amprphous semiconductors is the relaxation of the wave vector conservation rule that apply to optically

induced transitions in crystalline materials. Equation (3.4) is generally used for a-Si:H alloys with m = 2 and implicitly assumes parabolic bands and equal matrix elements for all optical transitions for photon energies in excess of the band gap [37] . It has also been reported that the better fit to the data is obtained when m = 3 [$g(E)$ linear dependence on E] is used [38].

3.3 Defects

In a-Si:H and related alloy films, defects play the important role in determining their properties. Dominant defects in these films are believed to be dangling bonds. The dangling bond is defined as the constituent atom which has the coordination number smaller by one than the normal coordination number. Therefore, it has an unpaired spin when it is not charged. One can determine the density of neutral dangling bonds by electron spin resonance (ESR) measurements[16]. ESR signals can be expressed by the following resonance conditions:

$$g\mu_B H = h\nu$$

where μ_B is the Bohr magneton, H is externally applied magnetic field, h is Planks constant, ν is the microwave frequency and g is a constant called g - value .

3.4 Relation Between Hydrogenation and Defects

The density of neutral dangling bonds in a-Si without hydrogenation is known to be around 10^{20} cm^{-3} , but by hydrogenation it is possible to reduce the density to about 10^{15} cm^{-3} [16]. Usually around 10 at. % H is needed to reduce the dangling - bond density to such extent . Fourfold - coordinated a-Si has a small structural flexibility resulting in a large stress Si network structure. This fact should be an important origin of the presence of a large density of dangling - bonds in a-Si without hydrogenation. Hydrogenation effectively reduces the coordination number to make the structure more flexible.

Hydrogenated amorphous Silicon , a - $Si_{1-x}H_x$ has an average coordination number $Z = 4-3x$, so that a typical concentration of 20% hydrogen decreases Z from 4 to 3.4, thus inducing a considerable reduction in overall strain. This reduction manifests itself not only by

minimization of the large scale imperfections but also by the sharp decrease in local distorted bonds and defects.

In addition, the Si - H bond strength is approximately 3.4 eV, about 40% greater than the Si - Si bond strength. Since H is more electronegative than Si tight binding calculation indicates that the Si - H bonding states are deep in the a - Si:H valence band, while the Si - H antibonding orbitals are not too far from the conduction band mobility edge (see figure 3.1).

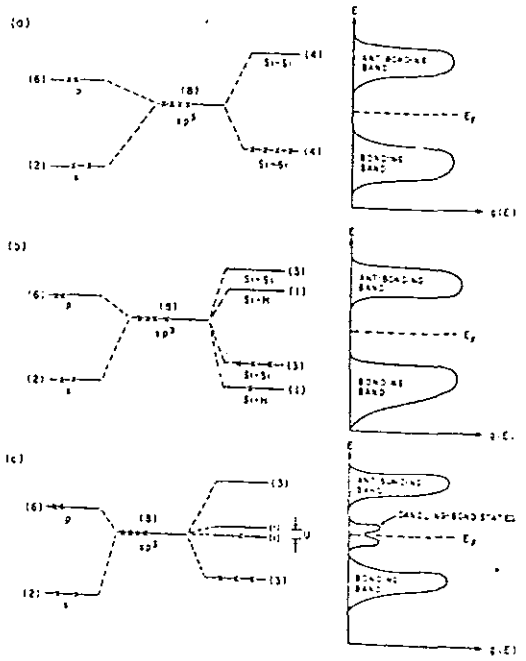

Figure 3.1 Tight - binding approach to the band structure of a-Si:H films : (a) a central Si atom is tetrahedrally coordinated by four neighboring Si atoms; the eight sp3 hybridized orbitals are split into four bonding and four antibonding orbitals , which repectively spread in to the valence and conduction bands of the solid . (b) A central Si atom tetrahedrally coordinated by three neighboring Si atoms and one H atom ; the Si-H bonding orbital falls deep within the valence band , while the Si-H antibonding orbital lies near the lower edge of the conduction band . (c) A central Si atom surrounded by only three neighboring Si atoms forming hybridized sp3 bonds . The fourth electron on the central atom occupies a nonbonding orbital (a dangling bond) , separated from its unoccupied partner by the correlation energy U , both non bonding states lie within the gap [17].

3.5 Density of States

Figure 3.2 sketches the density of electron energy states g(E). This is essentially the distribution of energy states of the CFO model [18] that has been proposed by Cohen Fritzsche, and Ovshinsky in 1969.

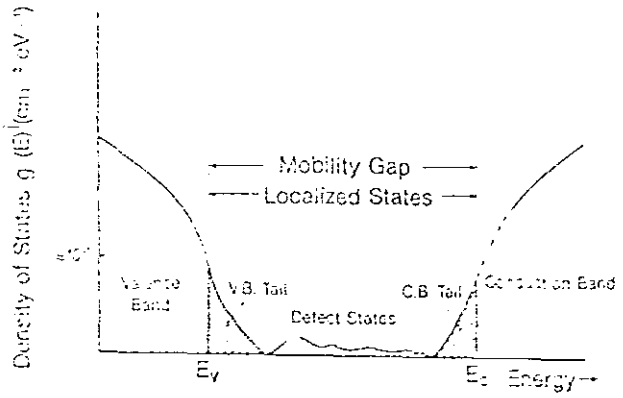

Figure 3.2 Band model of a noncrystalline semiconductor . E_v and E_c are the mobility edges of the valence band and of the conduction band , respectively[19] .

Both the conduction band and the valence band have tails of states and deeper in the gap there are states originating from structural and coordination defects (atoms which are not bonded according to their normal valency) as well as from impurities. Hence in contrast to crystals, g (E) is nowhere zero.

It is believed that the tail states are unavoidable because they are intimately associated with the disorder in noncrystalline structure. The valence band tails are covalent bonds that are weaker than normal. This can happen, for instance, when the covalent angle is bent from its equilibirium value, or when the bond is stretched due to internal strains. Moreover it was recently found, both theoretically and experimentally that there are net static charges on some atoms or groups of atoms [20]. These produce potential fluctuations which push states up and down and prevent any sharp feature in g(E). All these effects are expected to produce also a tail of states extending down in energy from the (antibonding) conduction band.

The total number of tail states is approximately 10^{-3} of the number of states in one band, and the number of defect - related gap states varies between 10^{-5} and 10^{-7} of band states [21] . This sounds like a very small fraction. Indeed, it is; but the requirement for device quality semiconductor materials are very stringent. One wishes, of course to have as few gap states as possible in order to control the electronic properties by intentional addition of donor and acceptor atoms. Furthermore, the gap states act as recombination centers of photoexcited charge carriers, and thus limit the photoconductivity and the life time of electrically injected carriers [22].

3.6 Optical Absorption

In describing absorption processes in solids, it is possible to categorize the major phenomena under six headings. They are, in order of commonly encountered decreasing energy of the transition :

(1) Electron transitions from the valence band to higher - lying conduction band, characterized by continuous high - absorption processes with structure variations depending on the density of states distributions in the bands involved. The optical absorption is usually in the range 10^5 - 10^6 cm^{-1} .

(2) Electron transitions from the valence band to the lowest - lying conduction band with a minimum required energy of the forbidden band gap. The magnitude and variation with energy of the absorption constant depends on whether the transition involves a photon only (direct transition) or whether it involves both a photon and a phonon (indirect transition). The absorption constant decreases by many orders of magnitude as the photon energy drops below the band gap energy .

(3) Optical excitation producing a bound electron - hole pairs, known as an exciton, requiring less energy than to produce a free electron - hole pair by excitation across the band gap. The exciton can be thought of as a hydrogenic system, capable of moving and transporting energy through the crystal without transporting net charge. The electron and hole making up an exciton may be thermally dissociated into free carriers or may recombine with the emission of light or phonons.

(4) If imperfections are present in the crystal , they create energy levels that lie in the forbidden gap (see sec.3.5). Therefore at energies less than the band - gap energy it is still possible to excite electrons to the conduction band from imperfection levels occupied by the electrons, or to excite electrons from the valence band to unoccupied imperfection levels, each process giving rise to optical absorption. This absorption in turn comes to an end when the photon energy is less than the energy required to make a transition from the imperfection level to one of the bands. For very high imperfection densities, the corresponding absorption constant may have values as high as 10^3 cm^{-1} , but in general is considerably less. In hydrogenated amorphous semiconductors defect absorption is of the order of 1 cm^{-1} .

(5) Absorption of photons by free carriers, causing a transition to higher energy states within the same band to higher bands. This process can occur over a wide range of photon energies. It involves the absorption of both photons and phonons since both energy and wave vector must be changed in the transition. There is also an optical absorption due to free carriers acting collectively as a kind of " electron gas ", which is known as plasma resonance absorption .

(6) Absorption of photons in the excitation of optical mode vibration of the crystal, known as Reststrahlen absorption. This is the only one of the above six phenomena that does not involve electron transitions.

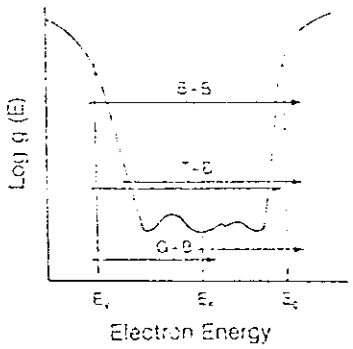

Figure 3.3 Optical absorption processes : B - B between extended band states ; T - B between tail states and band states ; and G - B between gap states and band states.

In Figure 3.3 the band model is plotted on a logarithmic scale in order to emphasize the relative magnitudes of band states, tail states, and gap states. Quantum statistics applies equally to electrons in noncrystalline and crystalline materials. Therefore, there is a Fermi energy E_F below which the energy states are occupied by electrons in equilibrium .

Essentially no electronic optical excitation can occur unless the photon energy exceeds a threshold energy that is large enough to lift an electron from E_v to an empty state above E_F or from an occupied state below E_F to E_c . These gap state to band state (G - B) transitions start at the threshold energy for photoconductivity. At higher photon energy, transition between tail states and band states (T - B) occur, and at even higher energy band to band (B - B) transitions take place .

The strength of the optical absorption is given by the logarithmic fraction of photons absorbed per cm of material . This absorption coefficient is proportional to the product of the density of those occupied states and the density of those unoccupied states that can be bridged by the energy of the incident photon, if the transition probability is the same for all states [23] .

Since the density of states g(E) of band tails and gap states differ so drastically, the absorption spectrum shown in figure 3.4 is expected. Strongest absorption is caused by B - B transitions ; G - B absorption is weakest and changes with g(E) of the gap states from sample to sample . The T - B absorption is nearly exponential suggesting that g(E) of the tail states falls off exponentially. The main objective of this experiment is the measurement of the B - B absorption coefficient as a function of temprature of a-Si:H thin films.

Figure 3.4 shows a typical plotting of the optical absorption coefficient α of a-Si:H against the photon energy E =hν. The optical absorption can be classified into three regimes [24] : (A) a band - to - band transition, (B) a transition between band tail and extended band states, and (C) a transition between defect and band states. In regime (A), α can be expressed as :

$$\alpha = B\frac{(h\nu - E_g)^2}{h\nu}$$

and such a plot is called the Tauc plot. Here E_g is defined as the optical gap and B is a proportionality constant which reflects the randomness of the network structure. In regime (B)

$$\alpha = \alpha_0 \exp(\frac{h\nu}{E_u}) \quad ,$$

and E_u is called the Urbach tail energy and is determined by the slope of the valence band tail . In such localized states, the carrier conduction is possible only through hopping, so the mobility is very small. Therefore, the boundary between such localized states and extended band states is called the " mobility edge ". The gap between the mobility edges in the conduction band and the valence bands is a "mobility gap" which corresponds to the band gap in crystals for carrier conduction.

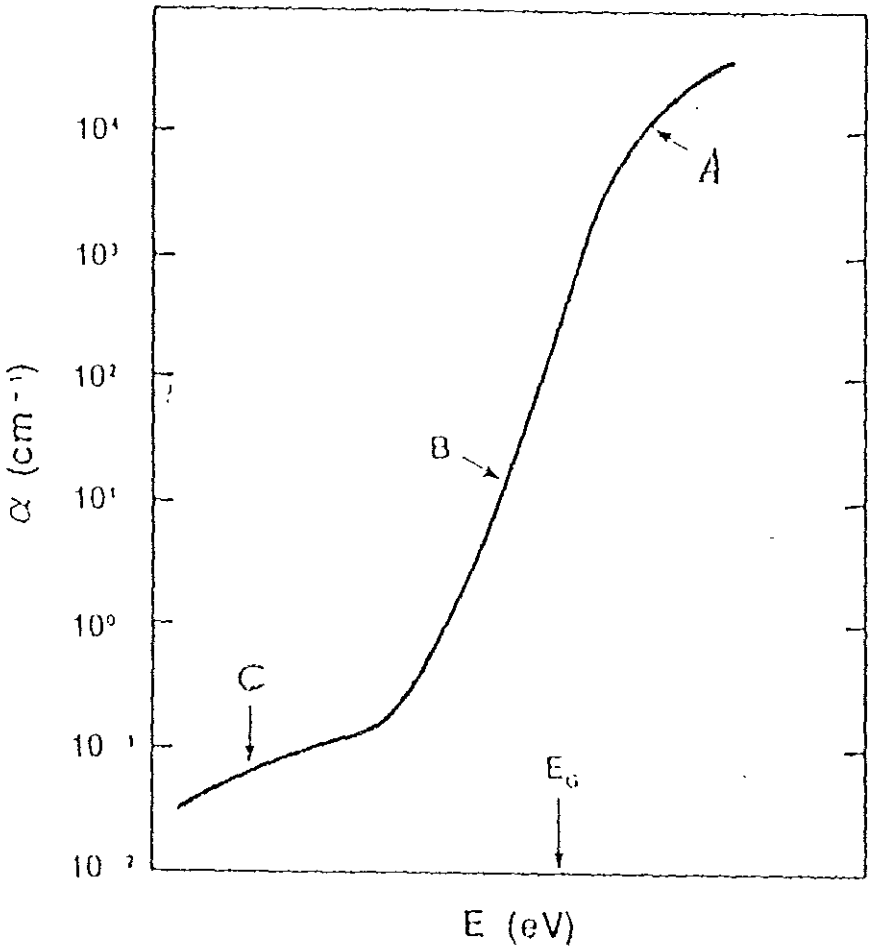

Figure 3.4 Typical features of the absorption coefficient α against the photon energy E=hν [46].

4 Temperature Dependence of the Energy Gap in Semiconductors

The variation of the energy gap with temperature is one of the fundamental problems in solid state physics. It is also a major problem in photovoltaics wherein solar cells are exposed to temperature varying conditions. It was suggested [25] that the following relation holds for the temperature dependence of the energy gap in semiconductors :

$$E_g = E_0 - \frac{\alpha T^2}{(T+\beta)}$$

where E_g is the energy gap which may be direct or indirect, E_0 is its value at 0 K, α and β are constants.

Most of the variation in the energy gap with temperature is believed to arise from the following two mechanisms :

(1) A shift in the relative position of the conduction and valence bands due to the temperature dependent dilation of the lattice [26,27] . Theoretical calculations [27] show that the effect is linear with temperature at high temperatures. At low temperatures the thermal expansion coefficient is nonlinear with temperature, correspondingly the dilation effect on the energy gap is also nonlinear.

(2) The major contribution comes from shift in the relative position of the conduction and valence bands due to temperature - dependent electron lattice interaction. Theoretical treatments [28-33] show that this leads to a temperature dependence of the following form :

$$\Delta E_g \propto T^2 \qquad \text{for} \quad T \leq \theta$$

$$\Delta E_g \propto T \qquad \text{for} \quad T \geq \theta$$

where θ is the Debye temperature .

On the other hand for a-Si:H, G. Weiser and H. Mell [43,45] formulated the variation of E_g with temperature to be :

$$E_g = E_g(0) - \beta\hbar\Omega n(\hbar\Omega)$$

where the Einstein - Bose distribution n ($\hbar\Omega$) of the optical phonons determine the temperature dependence β is the coefficient of the gap in units of the Boltzmann constant k. They reported [43] that the thermal shift of the absorption edge both in c-Si and a-Si :H is proportional to the density of optical phonons which in both cases could be represented by the same Einstein - Oscillator of about 33 meV and thereby confirmed interband mixing of valence and conduction band states. In the following section we will consider the experimental techniques used to determine the temperature dependent behavior of optical constants (energy gap, absorption coefficient) of layers of a-Si:H thin films.

5 Experimental Details

The aim of this experiment is to study the optical properties of different layers of a-Si:H films as a function of temperature. The spectral region of major interest for semiconductors is in the vicinity of the absorption edge, since it can provide information on the optical gap as well as on the density of states within the gap. For semiconductors such as a-Si:H, n and k are usually obtained from transmittance (T) and reflectance (R) measurements[39]. Therefore, in this work we want to see the variation of E_g and absorption coefficient α from near normal incidence transmittance and reflectance measurement in visible range of the spectrum (300-1100) nm as the temperature of a-Si:H films varied from (80-400) K. The experiment was carried out under vacuum condition (isolated system for thermal shielding) using cryostat; otherwise the optical constant of the sample environment for example its refractive index could vary. Light is incident on a-Si:H film with film side facing the illumination where the sample is fixed in the sample holder inside the cryostat at known temperature, the reflected and transmitted intensity is measured at each temperature using photodetector and from it reflectance and transmittance is calculated. In what follows we will consider the vacuum system, photodiode array system ,cryostat system and optical systems each separately in brief.

5.1 Vacuum system :

The main components of the vacuum system are : cryostat , vacuum gauge IE 211 with IONIVAC IM 210, TURBOVAC 50, frequency controller NT 50, prepump TRIVAC D4B and exhaust AF4 - 8. The principle of the operation is such that gas (air) is pumped out from the volume of the system to create vacuum pressure. The actual pressure reached is indicated by pressure gauge. At room temperature the lowest pressure reached was about 10^{-6} mbar (see diagram 5.1) .

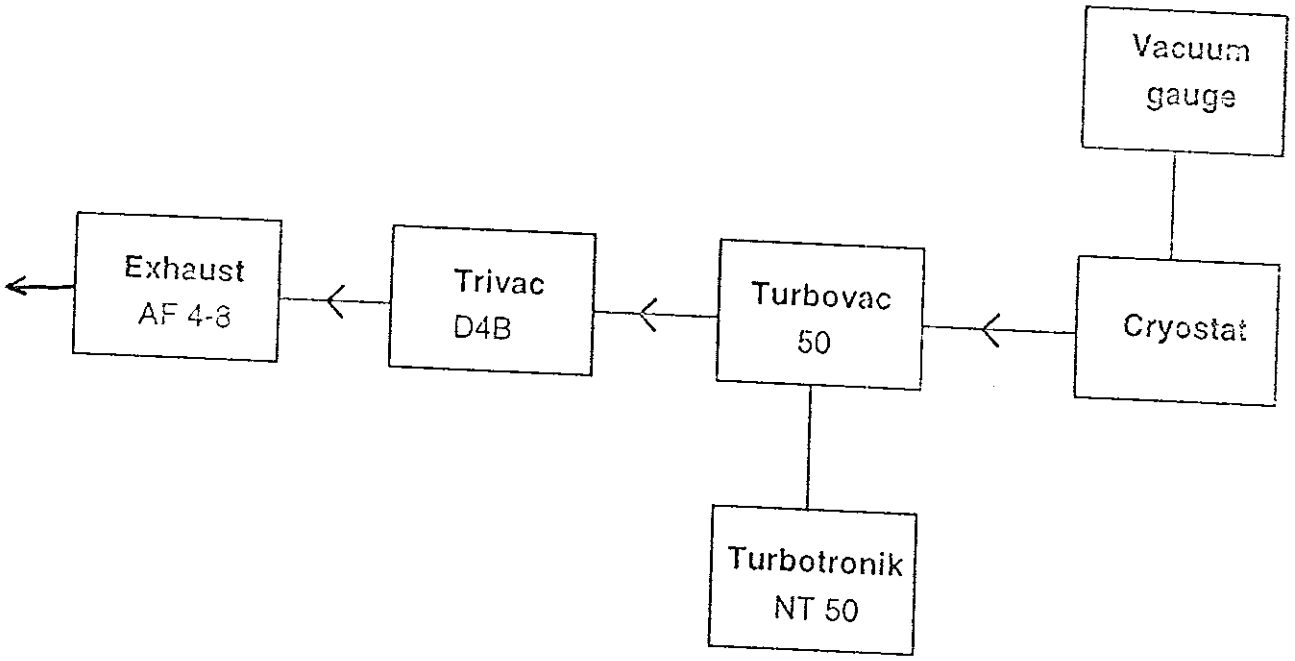

Figure 5.1 vacuum system (where the company specifications are also given).

5.2 Cryostat system

The temperature in the cryostat is controlled by using liquid nitrogen, heating system and platinum resistance thermometer (PT 100). Liquid nitrogen is tapped from one side of the cryostat, it circulates through it (through heat exchanger) and its outflow is controlled by an adjustable valve. There is also a heating unit connected to the cryostat so that one can increase the temperature of the system as desired . The PT 100 sensor is closely situated near the sample site so that the temperature of the sample could be accurately known. In this manner the temperature of the system was regulated in the range 80 - 400 K (range of measurement). The variation of the temperature during measurement was less than 0.2 K. To ensure good thermal contact, Silver fluid was used to fix the sample to its holder. The diameter of the sample holder is about 8 mm (see diagram 5.2) for temperature control). In the diagram when one wants to cool the system, liquid nitrogen from reservior flows through the cryostat under pressure when the pump is applied through N_2-exhaust connection on the cryostat. The flow rate is controlled by an adjustable N_2 exhaust valve connected to the pump. The cooling rate is proportional to N_2 flow rate. This way the cooling rate is controlled and the requried temperature is reached. The region around the sample is effectively cooled. When we want to increase the temperature we stop the pump and simply heat the system (heater placed near the sample site) to the desired temperature by applying the current. The current is "tuned" and automatically stops when the temperature reaches the "preset" value and shortly afterwards it oscillates about the "preset" value and finally the system will be in thermal equilibrium at the "preset" temperature.The sample and Aluminum film were fixed on the sample holder using silver fluid as contact as the arrangement in diagram (5.2b) for convenience of R and T measurement (for details see sec.5)

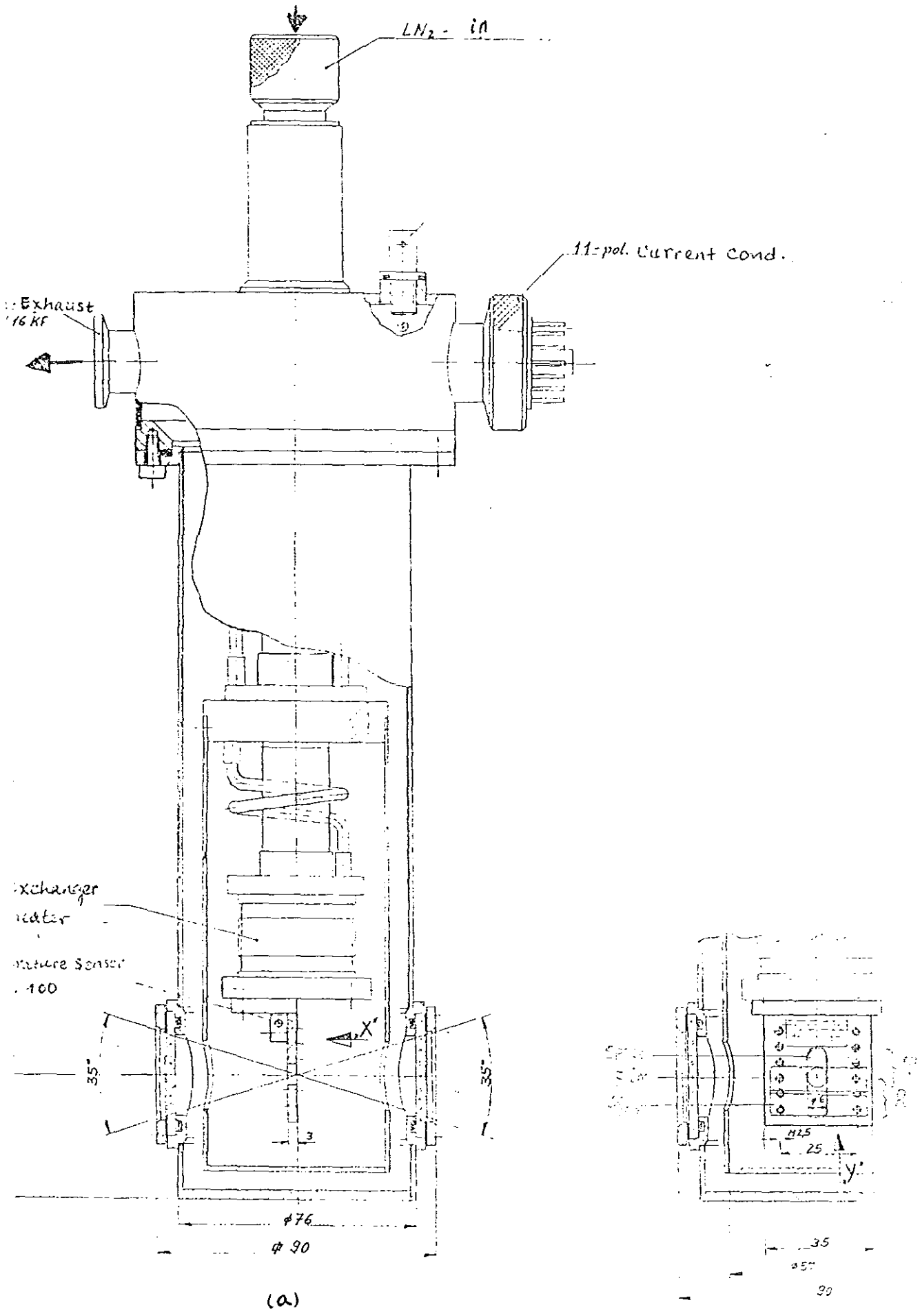

Diagram 5.2 (a) Temperature Control and (b) sample holder arrangement

5.3 Optical system :

For measurement of the transmittance and reflectance of the sample at near normal incidence the following optical alignments (Figure 5.3) were used. For oblique incidence one has to consider s -, and p - polarizations separately [41]. The light sourse used was halogen lamp. We used Koehler's principle for illumination of the sample in order to vary the "spot size" (2 - 6) mm and intensity independently at the sample site (center of the cryostat); for details see sec.5.3.1 . Neutral filters were also used when required to adjust the light intensity to the measurable range of the detector. The schematic drawing of the optical system is indicated in figure 5.3 .

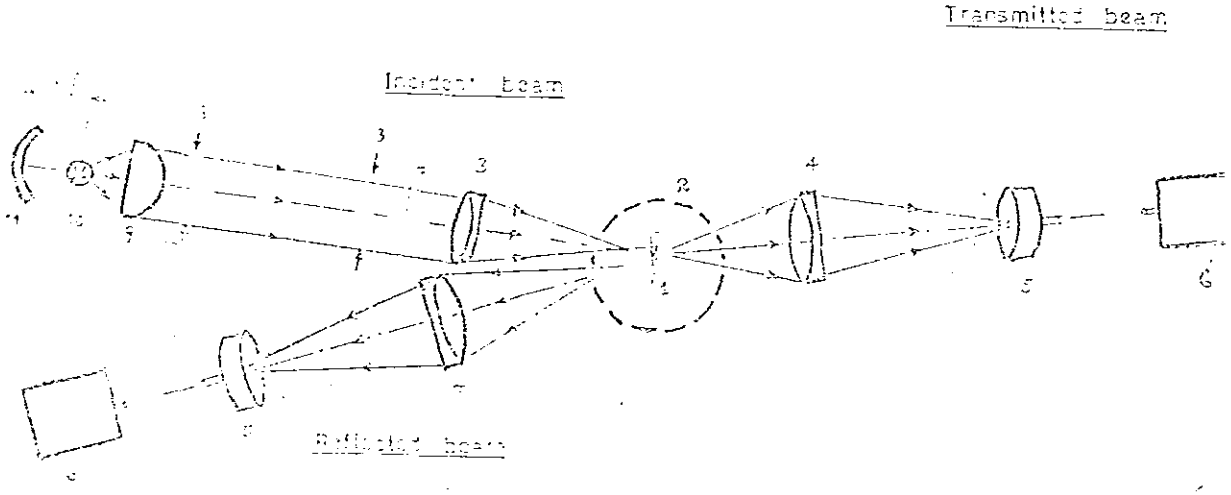

1 - Sample
2 - Cryostat
3 - Lens ; f = 50mm
4 - Lens , f = 30mm
5 - Optical fiber adaptor
6 - Detector
7 - Intensity filter
8 - Diaphragm
9 - Spherical lens
10 - Halogen lamp filament
11 - Reflecting mirror

Figure 5.3 The optical system

5.3.1 Details of the illumination technique

The filament of the halogene lamp is placed at a distance of 24 mm from the first lens L1 (Figure 5.4). The first diaphragm (field stop) is placed at a distance of 39 mm from the filament. The image of the filament is 5 times magnified and formed at a distance of 144 mm from the filament. Here we have placed a second diaphragm (aperture stop). A second lens is placed a distance equal to its focus i .e. 40 mm from the aperture stop. Our goal is to vary the intensity and the spot size independently at the object plane. This in essence is the Koehler's principle. We need to vary the spot size as our sample holder has limited diameter d = 6 mm and we need to vary the intensity as our detector has a 12 bit A/D converter. Consider now the effect of reducing the diameter of the field stop (Figure 5.5) as compared to the reference one (Figure 5.4); the image of the filament does not change but we reduce the spot size at the object plane. Again consider the effect of reducing the diameter of the aperture stop without changing the field stop diameter (Figure 5.6); the effect is to reduce the intensity of the light at object plane without changing the spot size (compare with Fig 5.4). This is so because we have reduced the solid angle of illumination. In other words, we have reduced the numerical aperture NA of the system. Thus, using the above approach we controlled the sample illumination .

Fig 5.4

Influence of Field stop (1)

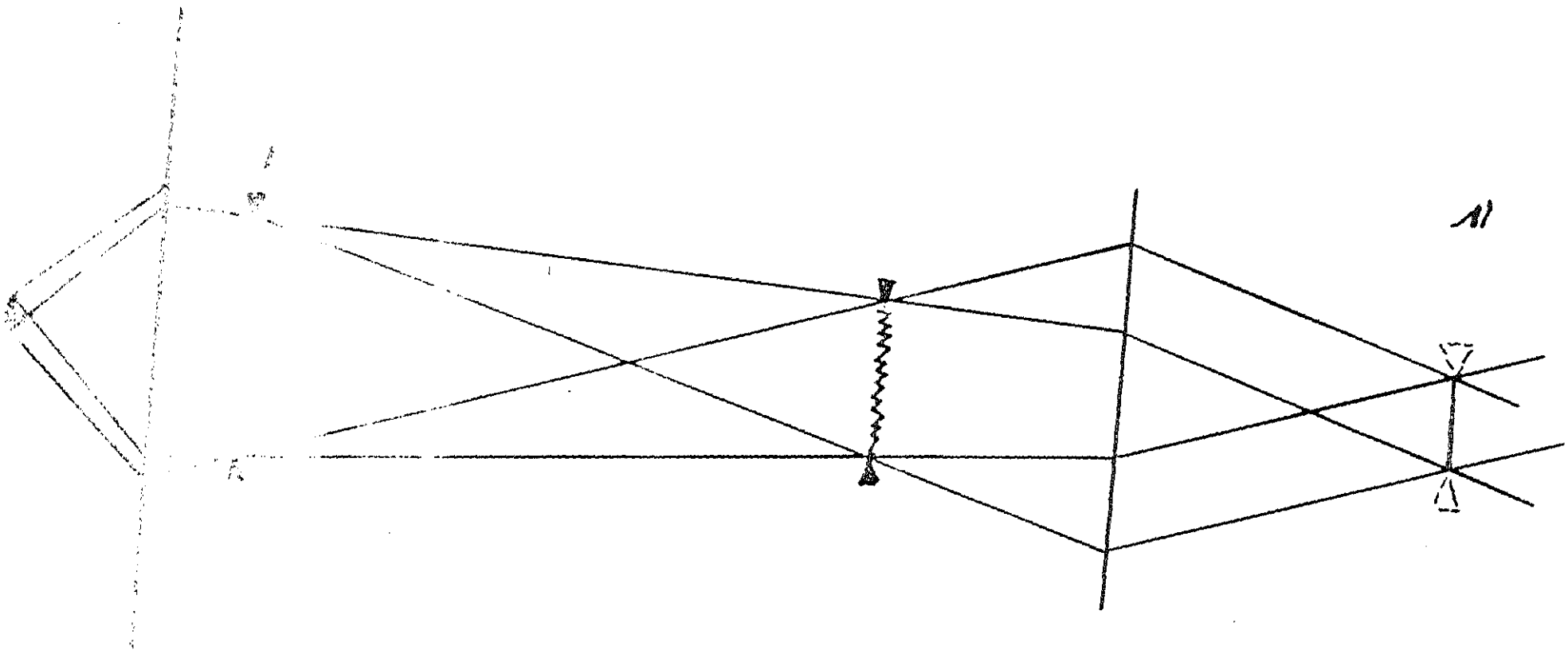

Figure 5.5

Influence of Aperture Stop (2)

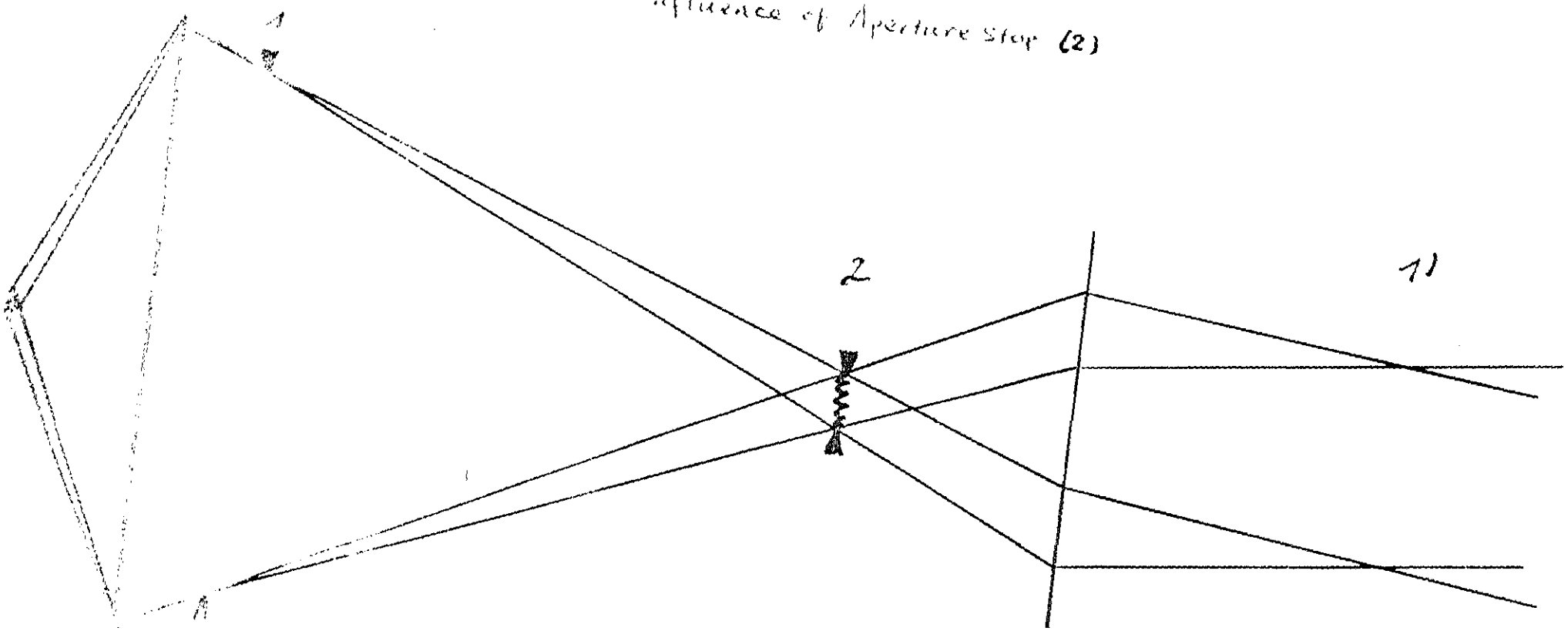

Figure 5.6

5.3.2 Collecting optics

In this section, the technique used to optimize the numerical aperture NA of the optical fiber to the divergence of the beam, focal length and diameter of the commerically availble lens is discussed. As it is known, for light to be transported through the optical fiber and reach the detector, it must be incident on the fiber within the solid angle corresponding to its numerical aperture; otherwise it will be attenuated and does not fully reach the detector. Therefore, this optimization is very essential.

consider Fig.5.7 ; indicating light diverging from the sample and collected by lens to the fiber.

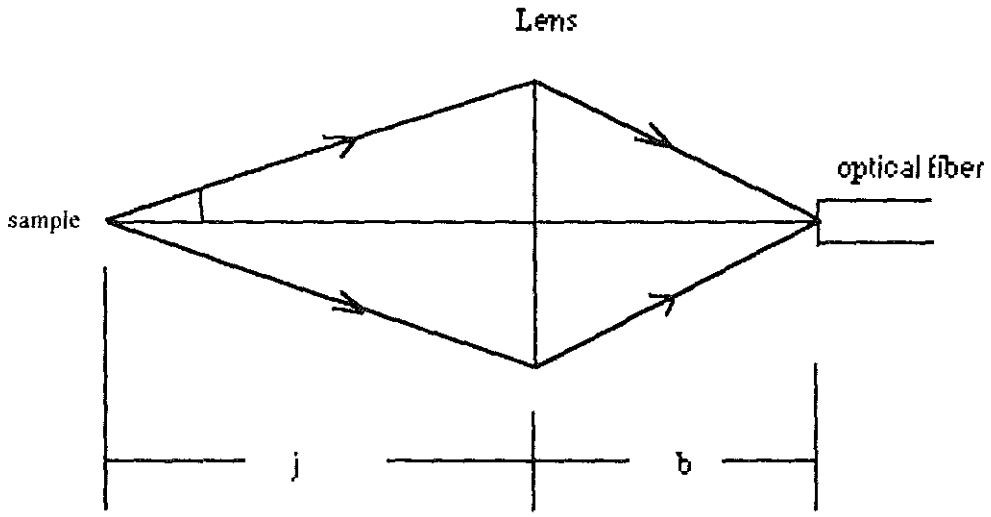

Figure 5.7

We used the distance j = 100 mm; the numerical aperture of the fiber is NA = 0.2 and its diameter is 0.5 mm. Now for magnification of 0.4, with the diameter of the spot size at the fiber of 2 mm (overfilled fiber head) and with maximum angle of divergence of the beam of 4 degree, we have the numerical aperture of the system $NA = \tan\beta = \frac{l}{b}\tan\alpha = 0.18$. This is close to the optimal value .

The focal length of the required lens is , from the thin lens formula $f = \frac{jb}{j+b} = 29mm$. But the commercially available lens is of 30 mm focal length. To calculate the diameter of the required lens consider the diagram below.

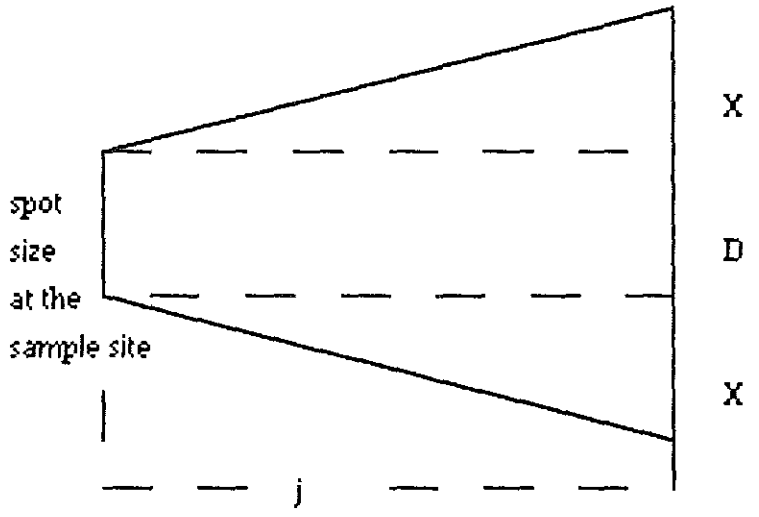

Figure 5.8

for $\tan\alpha = 0.07$, ($\alpha = 4$), the diameter of the lens is given by $2X + D = (2j\tan\alpha + D)$. and D = 5 mm, we get lens diameter of 19 mm and for D = 2 mm, we get the diameter of the lens

to be 16 mm . But for tan α = 0.05 (α = 3), and for D = 5 mm, we get for the diameter of the lens 12 mm and for D = 2 mm a diameter of 9 mm. So if we limit the primary divergence to α = 3 and the spot size to less than 5 mm, a commerically available achromat lens with f = 30 mm, diameter 11.5 mm, will fit to our need.

5.4 Photodiode array system

The detector is a miniature spectrometer modul (CARL ZEISS , MMS) with interface and software. It has a built-in self - scanning photodiode array. A photodiode array is a line of silicon detectors constructed as an integrated circuit. Light generates photo-current and causes a charge to accumulate in a series of diodes. Switching transistor sequentially read and reset the charge from each diode element, and direct the output to a single output line. The output charges are converted to a voltage, amplified and converted by analog-to-digital converter into a series of digitalized readings for computer processing.

The cycle time for the scan of the diodes, along with the light intensity, governs the charge stored before it is read. The scan rate is determined by clock pulse which are fed to the array circuit by an external controller.

The most important advantage of photodiode arrays over other detectors such as photomultiplier tubes is the multichannel nature of the arrays. Many hundreds of data points (channels,wavelengths) can be recorded in one single reading. As a consequence, diode arrays are excellent for taking a series of scans of a changing optical source and take an entire spectra in a few miliseconds.

Diode arrays and photomultiplier tubes are fundamentally different in their method of light measurement. Unlike photomultiplier tubes which measure radiant flux (power) diode arrays measure radiant energy. The diode elements accumulate charge generated by the arrival of photons, and the charge is proportional to the total radiant energy. For constant light source, this is the product of the radiant flux and exposure time. In essence a diode array acts as an electronic photogrphic film and the exposure time is adjusted to obtain the best signal. Thus we set the integration time depending on the incident light intensity to get optimum signal from diode array system.

The spectral response of a silicon diode is that of silicon, and is from about 180 nm to 1100 nm, while ligt source was halogen lamp 300 nm to 1100 nm. Diode array systems ability to make many scans a second and to present the results graphically, with constant updating makes it useful tool for the adjustment of of the optical system. Changes in intensity, image size and position, and spectral distribution are immediately visualized. Laborious alignments of many hours can often be accomplished in a few minutes by suitabily placing the diode array and observing changes in signal shape on graphic dispaly.

Its measuring principle is as follows : Light is incident on a diffracting grating from left (Figure 5.9) through optical fibre.Light is "reflected" at the grating (reflection grating) and dispersed into different wavelengths. The photodiode arrays (with second order diffraction suppressed using appropriate wavelength filters) detects light incident on it. The Silicon photodiode responds to all photons with energy greater than or equal to its optical band gap. The wavelength interval was from 300 - 1100 nm for this measurement. The computer registers and stores the number of counts as a function of pixel (diode) number. The calibration certificate gives the least - square fit for wavelength as a function of pixel number. Using this relation one can obtain counts as a function of wavelength .

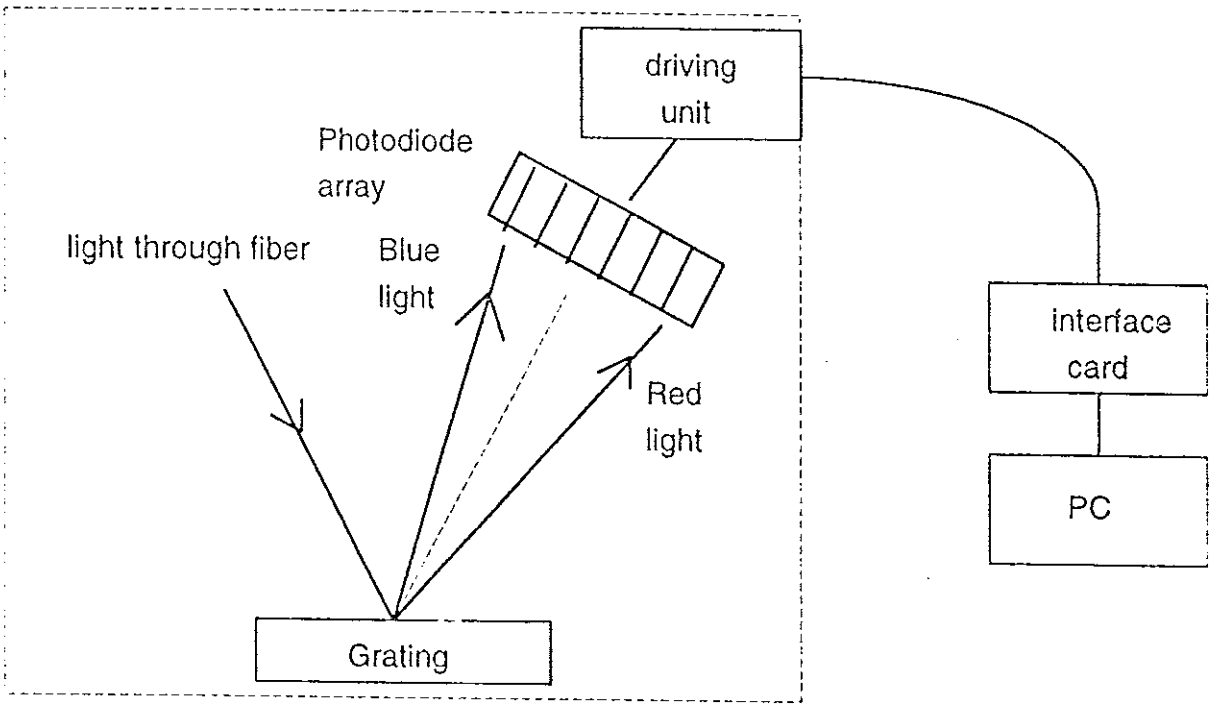

Figure 5.9 schematic drawing of the photodiode array system.

5.5 Sample preparation

In this section a short discription of sample preparation is give for the sake of completeness; otherwise the sample is prepared by ISI-PV deposition group led by Dr.Claus Beneking for which I am grateful.

a-Si:H thin films are prepared by "Plasma Enhanced chemical vapor Deposition" (PECVD). The concept of PECVD is derived from CVD - process, in which an appropriate gas is thermally dissociated in hot plate and leads to deposition of thin films. In CVD - process the required high deposition temperature leads to raised production cost and limits also the choice of substrate which is its maior setback.

On contrary, in PECVD - process through an additional plasma the deposition is enhanced so that the deposition temperature is considerably lowered. The standard deposition temperature for amorphous silicon by PECVD is about 200 celcius whereas for CVD - deposition of a-Si:H a minimum of 500 celcius is required.

The plasma used for deposition of a-Si:H film is only weakly ionized. The high energy electrons can transfer its energy to the gas molecules by collision whereby the molecules either dissociate and form radicals which leads to deposition or simply stay in the excited form. In order to avoid the cooling down of electrons and thus the disapperance of plasma, the plasma must absorb energy continuously. This happens through the electric field, which accelerate the electrons.

Films with few micrometer thickness need substrate for its mechanical stability. For this purpose Corning glass is used.

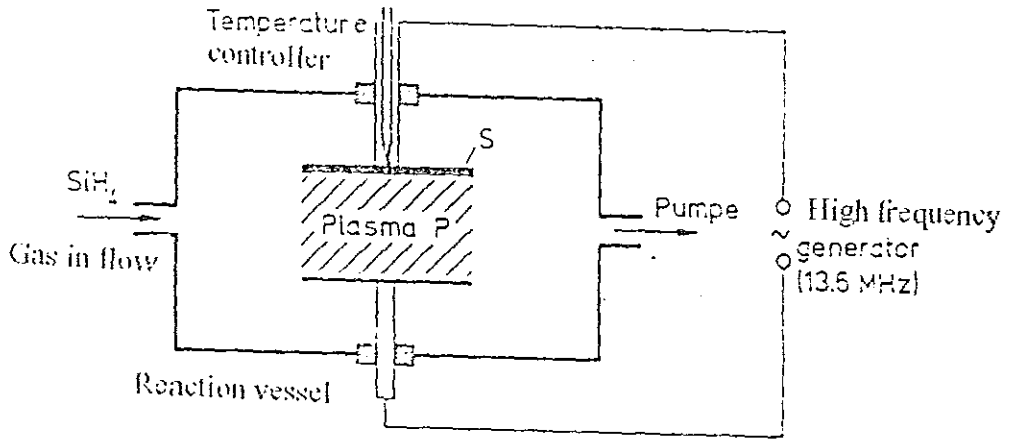

Figure 5.10 schematic diagram of a-Si:H film deposition system [8].

Figure (5.10) illustrates the plasma deposition principle of amorphous silicon. Silane (SiH_4) is continuously pumped into the reactor. Silane is decomposed by glow discharge between the two electrodes. From the depcomposition products undoped or intrinsic layer a-Si:H film is formed. For p-doping the process gas diborane (B_2H_6), and for n-doping phosphine (PH_3) is mixed in few concentrations with silane.

The thickness of a-Si:H films was accurately determined from interference pattern (R and T) curve obtained from experimental data and interference patterns obtained from calculations using the exact expression from the single layer structure based on known (Standard) optical constants using the optical simulation programme[40].

We also measured the thickness of the films by using Dektak 3030. The basic principle of its measurement is that the film wiil be first etched from the substrste and when scanned it would enable us to measure the thickness of the film. The structure of the surface to be scanned looks like"ㄱ".

5.6 R and T measurement

As mentioned previously, the temperature dependent optical constants of p - , i - , n - layers of a - Si:H films were determined from the temperature dependence of reflectance R and transmittance T measurements. We performed the R and T measurements in the temperature range of 80 to 400 Kelvin . Since the maximum temperature during our measurement was 400 K (less than the deposition temperature of a-Si:H), our measurement is in the reversible range.If the temperature is greater than the deposition temperature the film starts to loose its amorphous property [7].

5.6.1. Transmittance measurement

The transmittance T at various temperatures was measured using the following steps .

- We have set the temperature of the system to the required value using liquid nitrogen ,heating system and adjustable valve together with the nitrogen exhaust pump . We have waited until thermal equilibrium is reached ($\delta T \leq 0.2$ K) .

- we adjusted the " spot size " and the intensity of the illumination (non - saturation mode of the detector) without sample and we measured the intensity I_0.

- we measured the transmitted intensity I_t from the sample (sample adjustment was done by cryostat holder (manufactured at workshop) for both R and T measurement). The cryostat holder was designed in such a way that it can be fixed on the optical table and one can roll it back and forth perpendicular to the incident beam along the rail to align it to the center of fixed incident beam. In addition it can be moved up and down perpendicular to the plane of the optical table to center the sample with the incident beam. Moreover, the orientation of the plane of the sample can be finely adjusted for the incident light to be normally incident on it within +/- 5^0 angle. The cryostat can also be fully withdrawn from the beam to optimize the incident (reference) beam.

- Then the transmittance is calculated as $T = \frac{I_t}{I_0}$, where I_t and I_0 are transformed into counts as a function of wavelength by the transformation equation from the manufacturer of the detector .

5.5.2 Reflectance measurement

We followed the steps below for reflectance measurement. We used Aluminum film deposited on corning glass as reference reflector .

- We calibrated the reflectance of Al/Glass film using Perkin - Elmer Lambda 19 UV/VIS /NIR double beam spectrophotometer, at room temperature. After calibration correction is done we obtained R_{Al} . We assumed that $\frac{dR_{Al}}{dT} \cong 0$ for this temperature range .

- Then we fixed Al /Glass film on the sample holder with orientation of the film towards the illuminator.

- Adjacent to that we placed our sample and we left empty space above Al /Glass for transmittance reference intensity measurement .

- We measured the reflected intensity from Al / Glass I_{Al} and we measured the reflected intensity from our sample I_s at required temperature .

- Then the reflectance was given by $R = \frac{I_s}{I_{Al}} R_{Al}$.

6 . RESULT & DISCUSSION

The a-Si:H films used in our work were produced by a widely used plasma - enhanced chemical vapor deposition (PECVD) technique using rf (13.56 MHz) glow - discharge decomposition of silane. The films were prepared by ISI - PV deposition group. From measurement of Reflectance R and transmittance T depending on temperature, we have calculated the absorption coefficient α at different temperatures using the Hishikawa relation [41] given by $\alpha = -\frac{1}{d}\ln(\frac{T}{1-R})$.

The reflectance R and transmittance T of p - , i - , n - layers at room temperature is shown in Figures 6.1. The spectral fringes on R and T curves of Figures 6.1 are due to the thickness of the films . The periodicity of the fringes is inversely proportional to the product of the thickness and the refractive index of the film. Obviously, the thickness of the films does not change with increasing wavelength. However, the refractive indices of the films are energy dependent . At lower energies, since the refractive indices of the films are decreasing with decreasing energy, the spectral fringe on the curves of R and T are getting broader with decreasing energy .

The reflectance curve of all layers above 2.2 eV show a tendency to increase, whereas the transmittance curves go to zero. Transmittance is strongly connected with penetration depth . The penetration depth of an absorbing material is equal to an inverse of the absorption coefficient [41] . Thus, since amorphous materials have high absorption coefficient, the transmittance of the layers above 2.2 eV are negligibly small to be detected .

For energy range between 1.5 and 2.2 eV , the amplitude of the spectral fringes on R and T curves are not equal because of the absorption of light in the layers. For E > 2.2 eV α increases still, but as T curve is zero one can not evaluate it with Hishikawa relation.This opaque region is the domain of ellipsometry where instead of measuring only intensities, one measures two quantities ψ and Δ which are respectively related to the ratio of the reflected intensities and the difference in phase shifts at reflection corresponding to the components of vibration parallel and perpendicular to the plane of incidence.

We note from the tails of the transmittance curves that p - layers stop transmitting at relatively higher energies . Thus a p - layer has more band - pass which allows much light to pass through and reach the active i - layer .

From the magnitudes of the reflectance curves, we note also that the reflectance of the p - layer is small as compared to the reflectance of i - and n - layers .

Figure 6.2 a shows the reflectance of i-layer a-Si:H film; d $\cong$ 1000 nm at different temperatures. From the figure, as the temperature increases the reflectance curve shifts towards lower energy (red shift). In the energy range of about 1.75 eV to 2.05 eV, the amplitude of the reflectance curve drops as temperature increases. Therefore ,one can say that the reflectance R decreases with increase in temperature in this energy range.

In figure 6.3 a, the transmittance T of i - layer a-Si:H film is shown for different temperatures . As it is clearly apparent, with increase in temperature, the transmittance curve shifts towards lower energy range.The maximum shift occurs near the optical energy gap regions. In region where absorption occurs, transmittance decreases with increasing temperature. The penetration depth also seems to be decreasing with increasing temperature.

Figure 6.4 shows the absorption coefficient α of i - layer and n - layer (calculated from Hishikawa relation) at various temperatures. Since R and T decreases in the fundamental absorption region with increasing temperature and generally R + T + A = 1 from energy conservation where A is the fraction of energy absorbed, we expect the absorption coefficient α to increase with increase in temperature. This same behavior is observed in our result. As the

temperature is increased, the curve of the absorption coefficient α in general shifts towards lower energy. At constant energy, absorption increases with increase in temperature. The same behavior was also observed for p - layer with regard to R, T, and α dependence on temperature.

Figure 6.5 shows E_{04} (the energy at which the absorption coefficient α is exactly 10^4 cm^{-1}) for p -,i -,and n - layers of a-Si:H films with d $\cong$ 1000 nm each as a function of temperature. E_{04} decreases non-linearly for each layer as the temperature decreases.The measured data points are indicated on the curve for each layers.The data points were fited with the fiting equation $y = ax^2 + bx + c$. We observed good fit for each layer. Moreover we fitted the data with Varshini's formula and we observed a good agreement.

Figure 6.6 shows Tauc's plot for different temperatures of measurement for the i - layer sample. From the figure one can conclude that the optical energy gap decreases when the temperature increases. The optical energy gap decreased from 1.76 eV to 1.64 eV as the temperature is increased from 100 to 400 K. The Tauc's curve shifts to lower energy range with increase in temperature and it has nearly the same slope parameter.

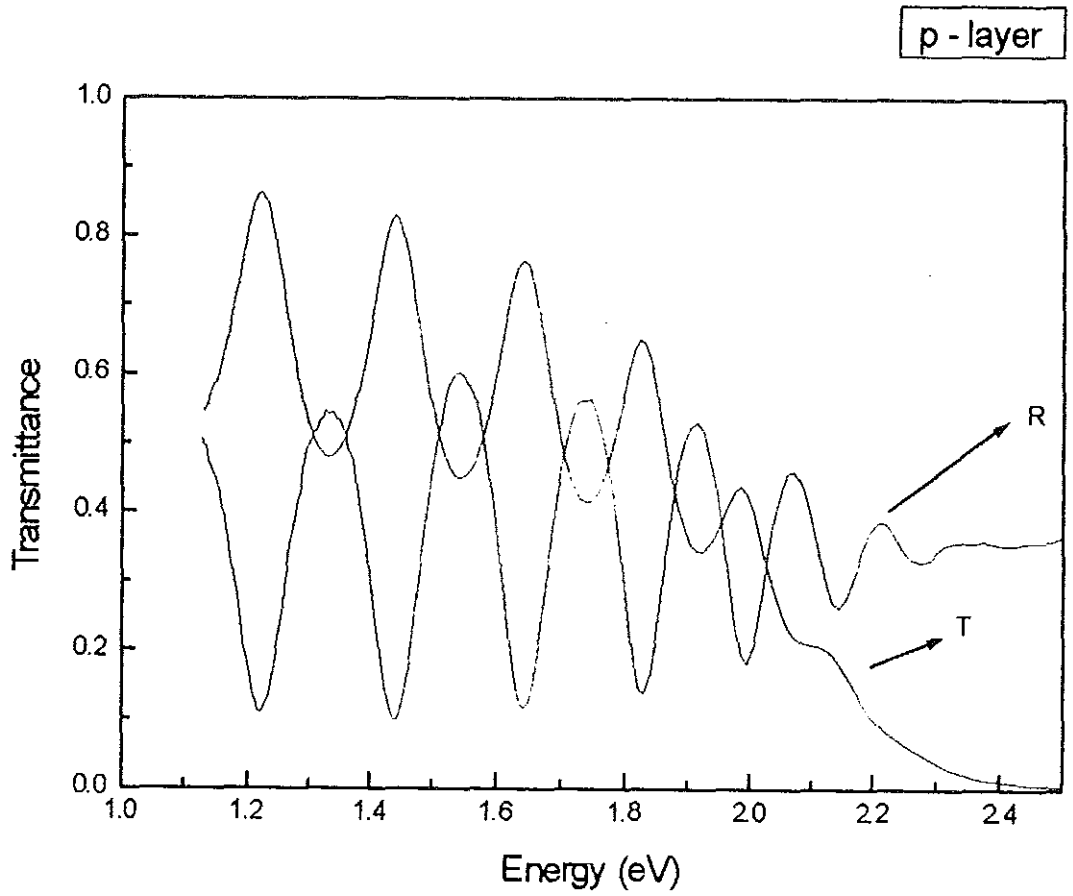

Figure 6.1 a Reflectance and Transmittance of p - layer a-Si:H film (94-110, d ≅ 1000 nm) at T = 300 K

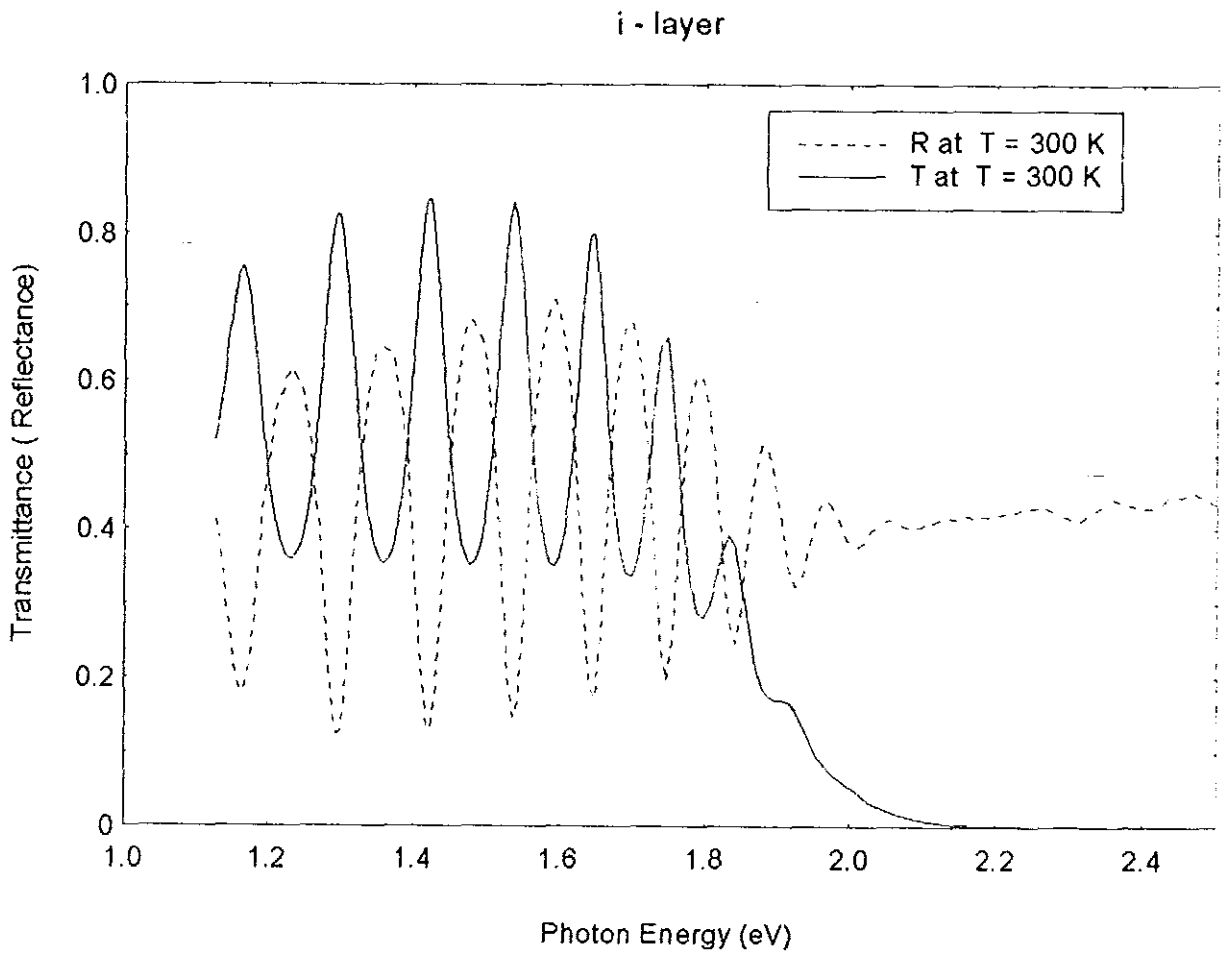

Figure 6.1 b Relectance and Transmittance of i - layer a-Si:H film (95-113, d ≅ 100 nm) at T = 300 K

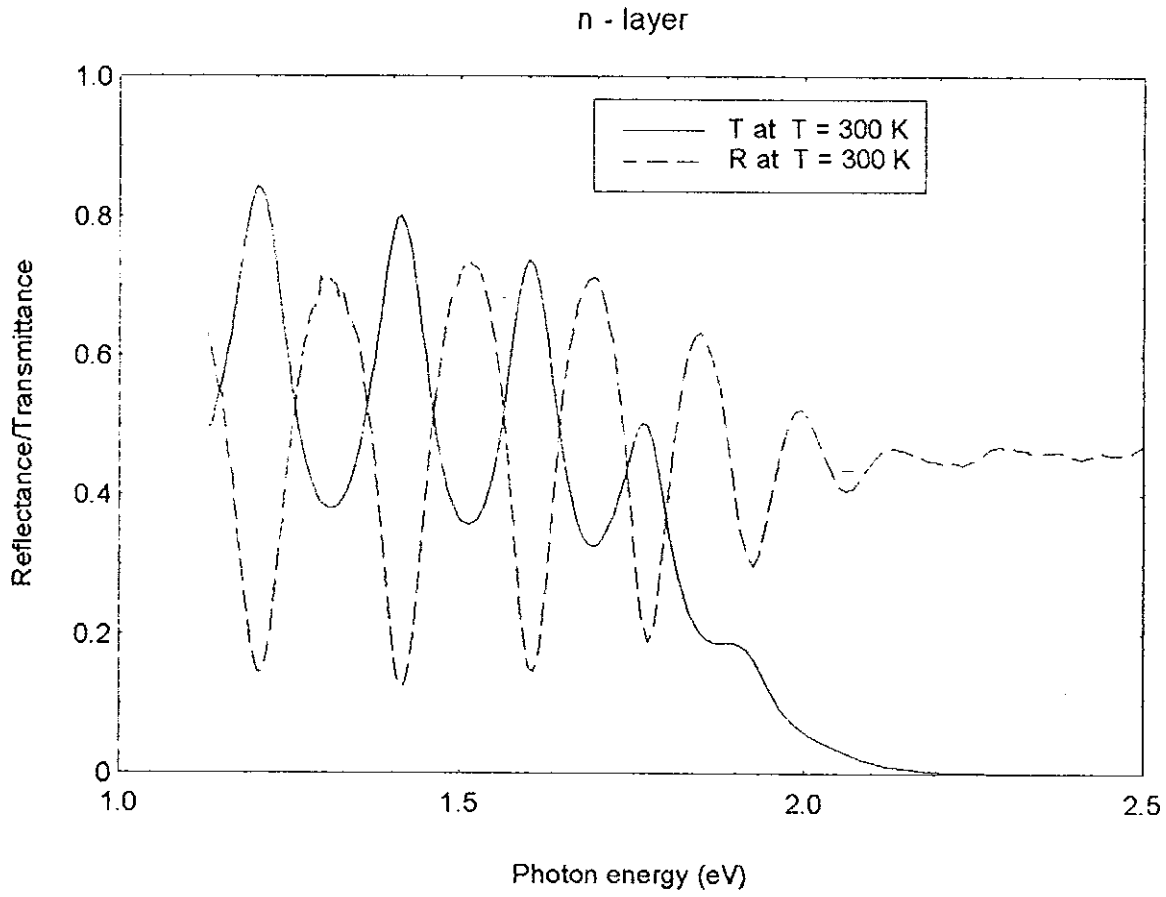

Figure 6.1 c Reflectance and Transmittance of n - layer a-Si:H film (95-212, d ≅ 1000 nm) at T = 300 K

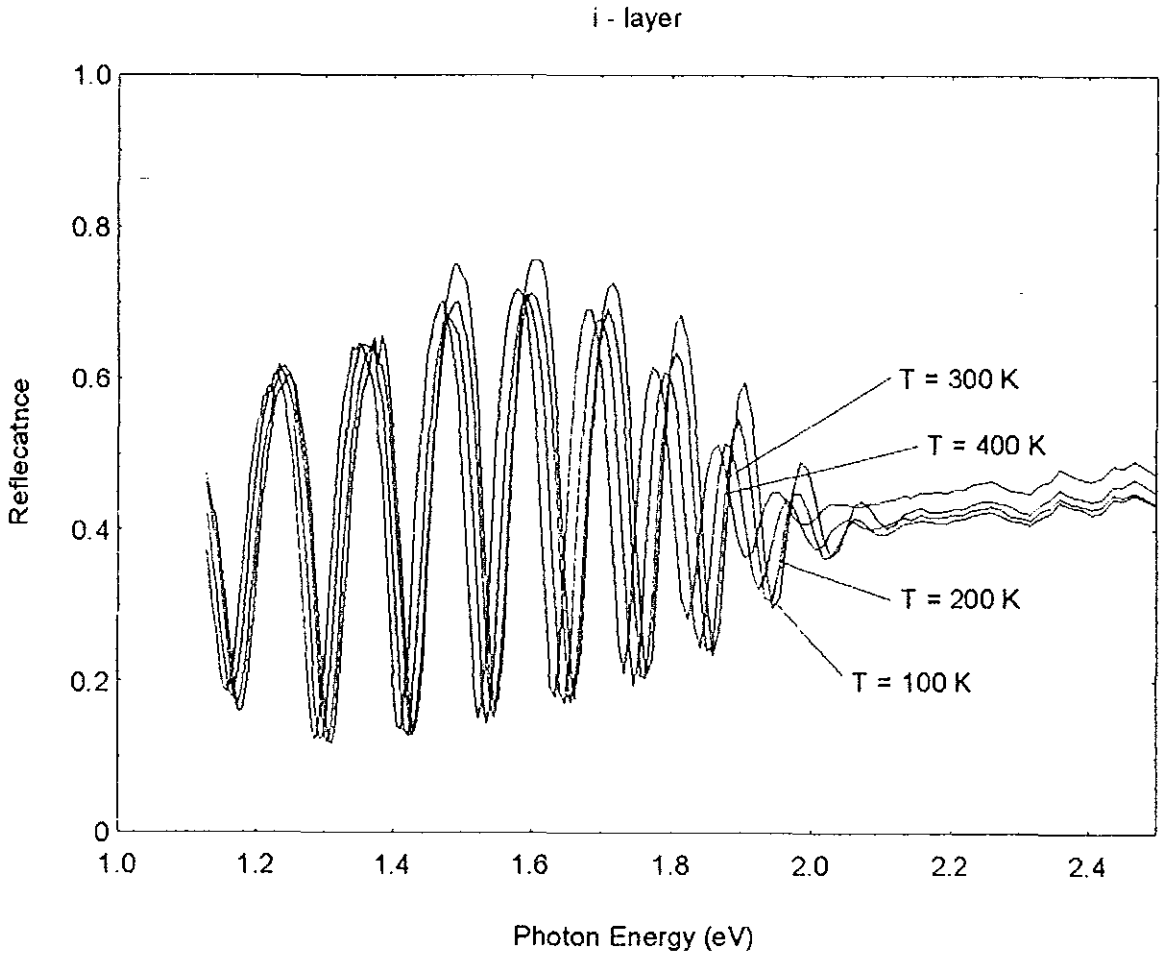

Figure 6.2 a Reflectance of i - layer a-Si:H film (95-113) at different temperatures. As temperature increases R-curve shifts towards lower energy range.

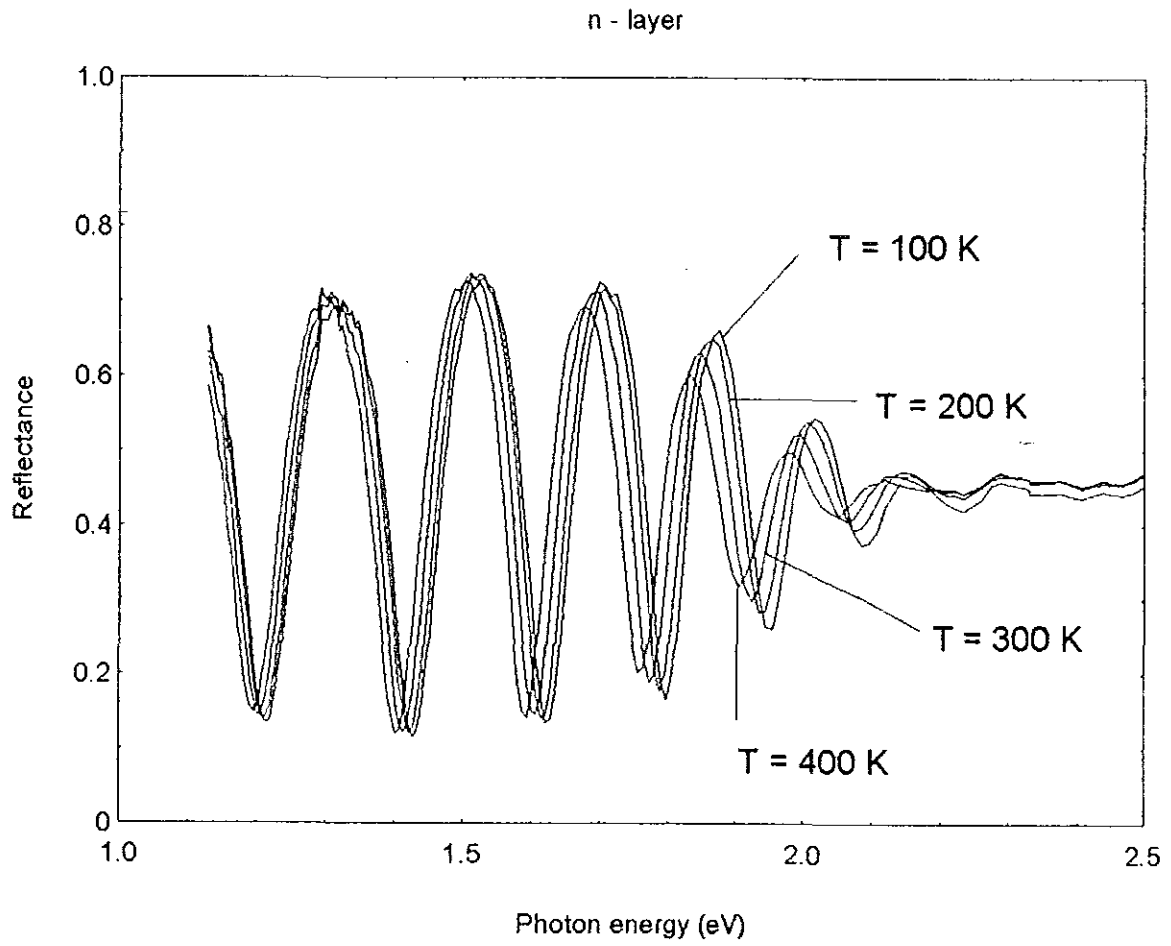

Figure 6.2 b Reflectance of n - layer a-Si:H (95-212) film at different temperatures. As temperature increases R-curve shifts toward lower energy range (red shift).

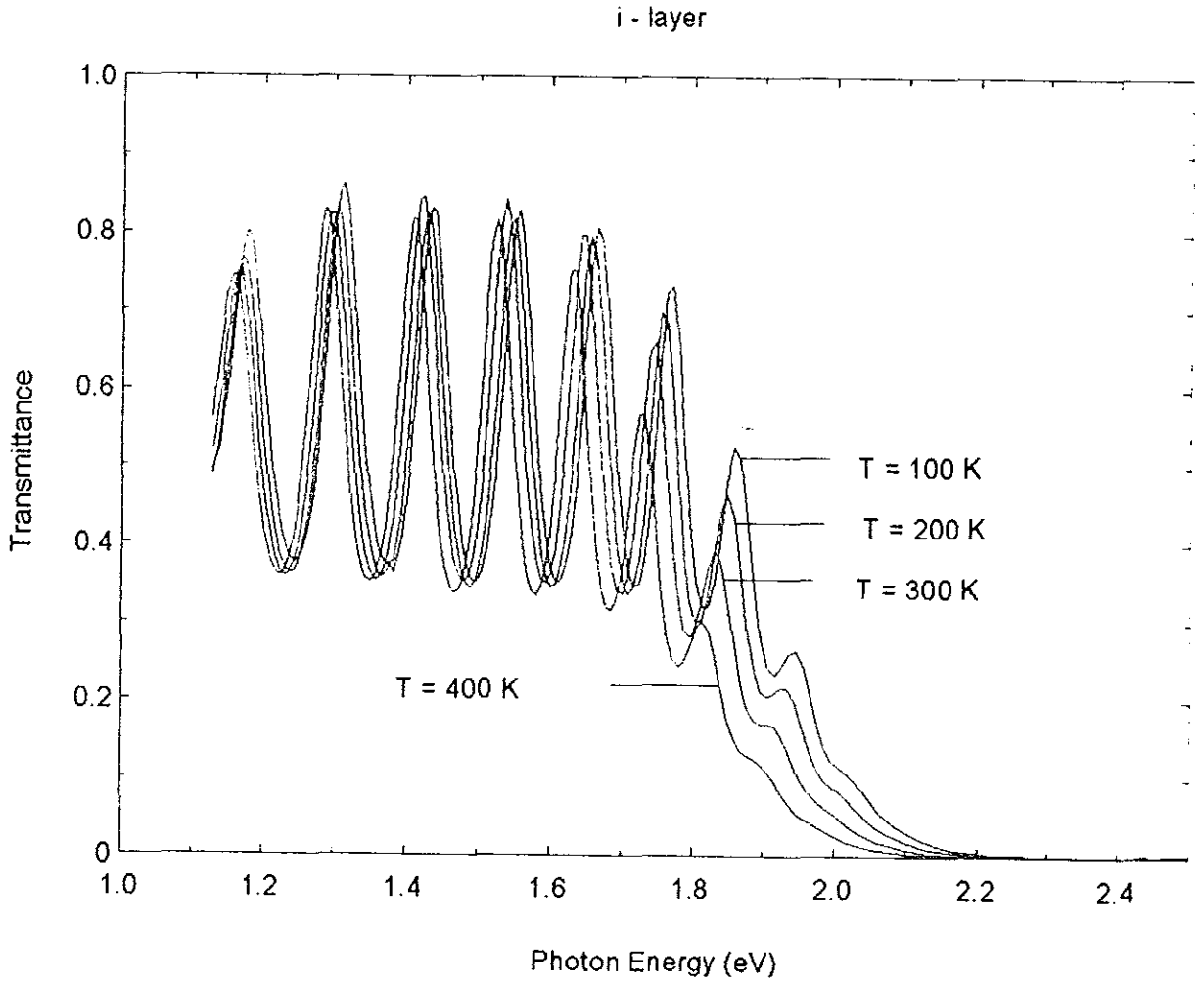

Figure 6.3 a Transmittance of i - layer a-Si:H (95-113) film at different temperatures. As temperature increases T-curve shifts toward lower energy range.

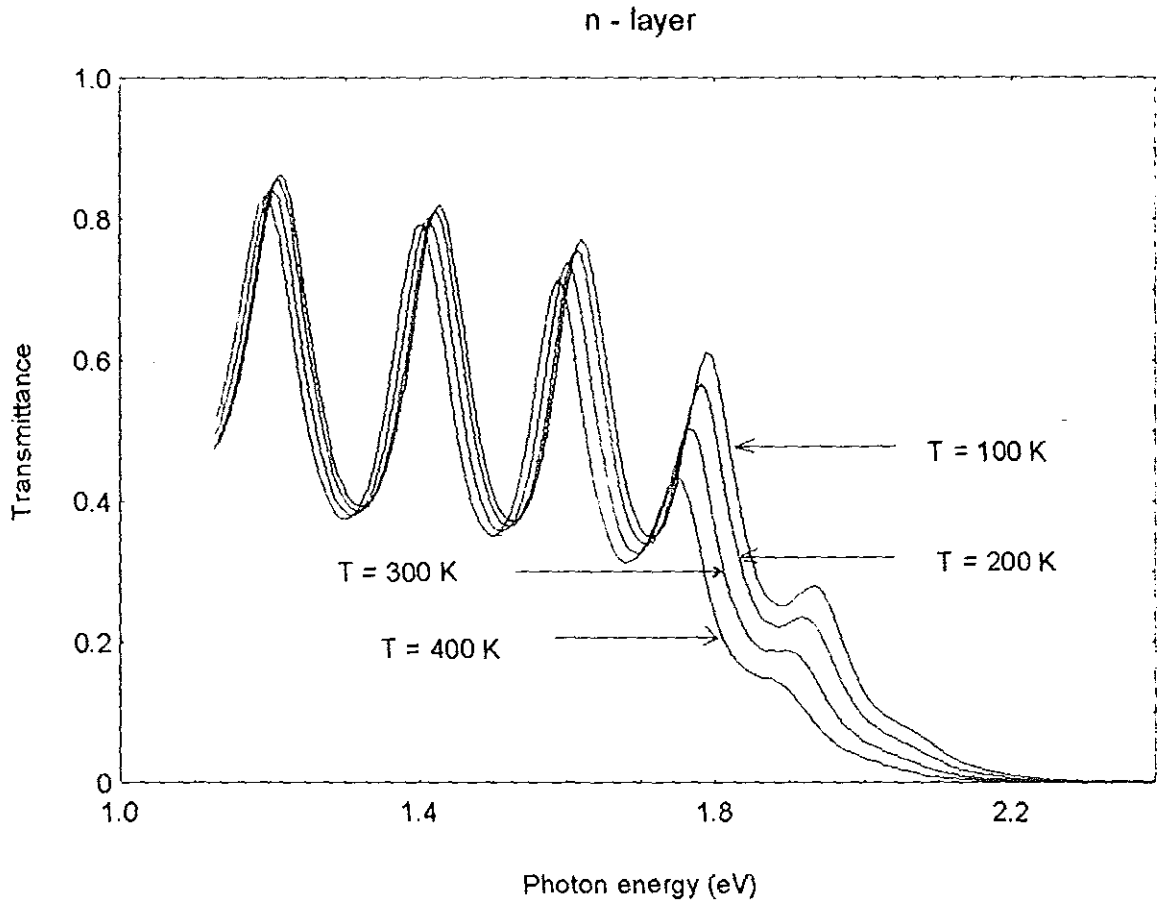

Figure 6.3 b Transmittance of n - layer a-Si:H (95-212) film at different temperatures. As temperature increases T-curve shifts toward lower energy range. The shift is maximum near the energy gap and is lower for energy far less than E_g .

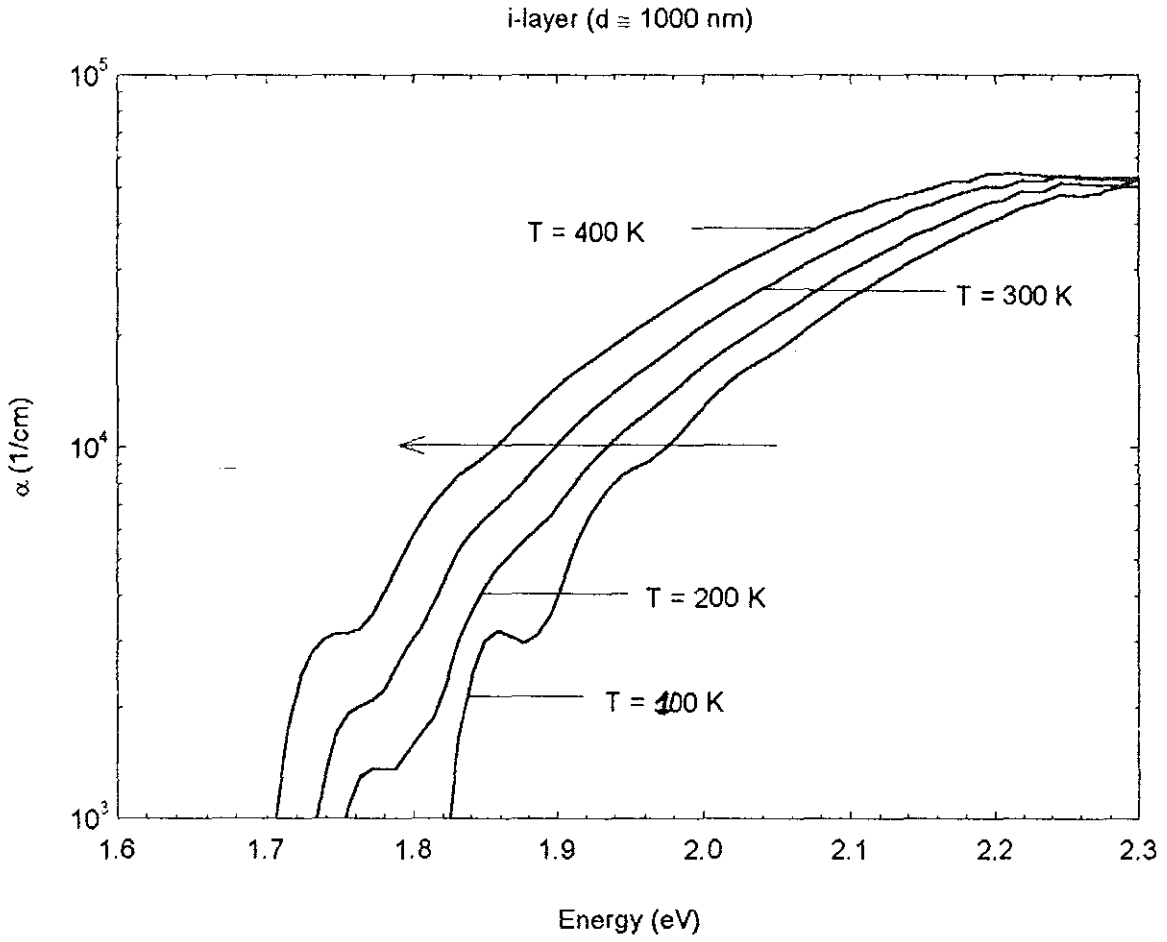

Figure 6.4 a α of i - layer a-Si:H (95-113) film at different temperatures. α-curve shifts toward lower energy range as the temperature increases. In other words, absorption increases for arbitrary but fixed energy when temperature increases.

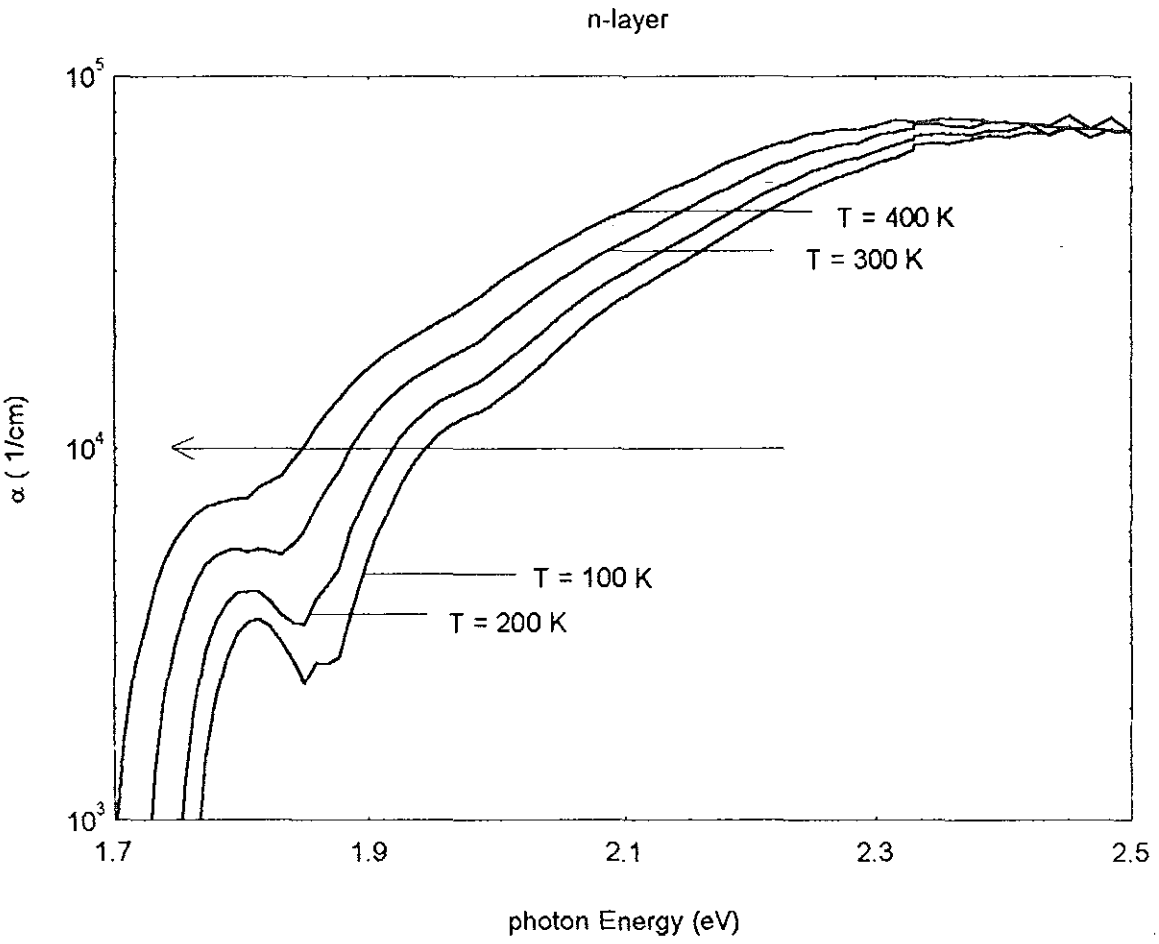

Figure 6.4 b α of n- layer a-Si:H film (95-212) at different temperatures. As temperature increases α-curve shifts toward lower energy range.

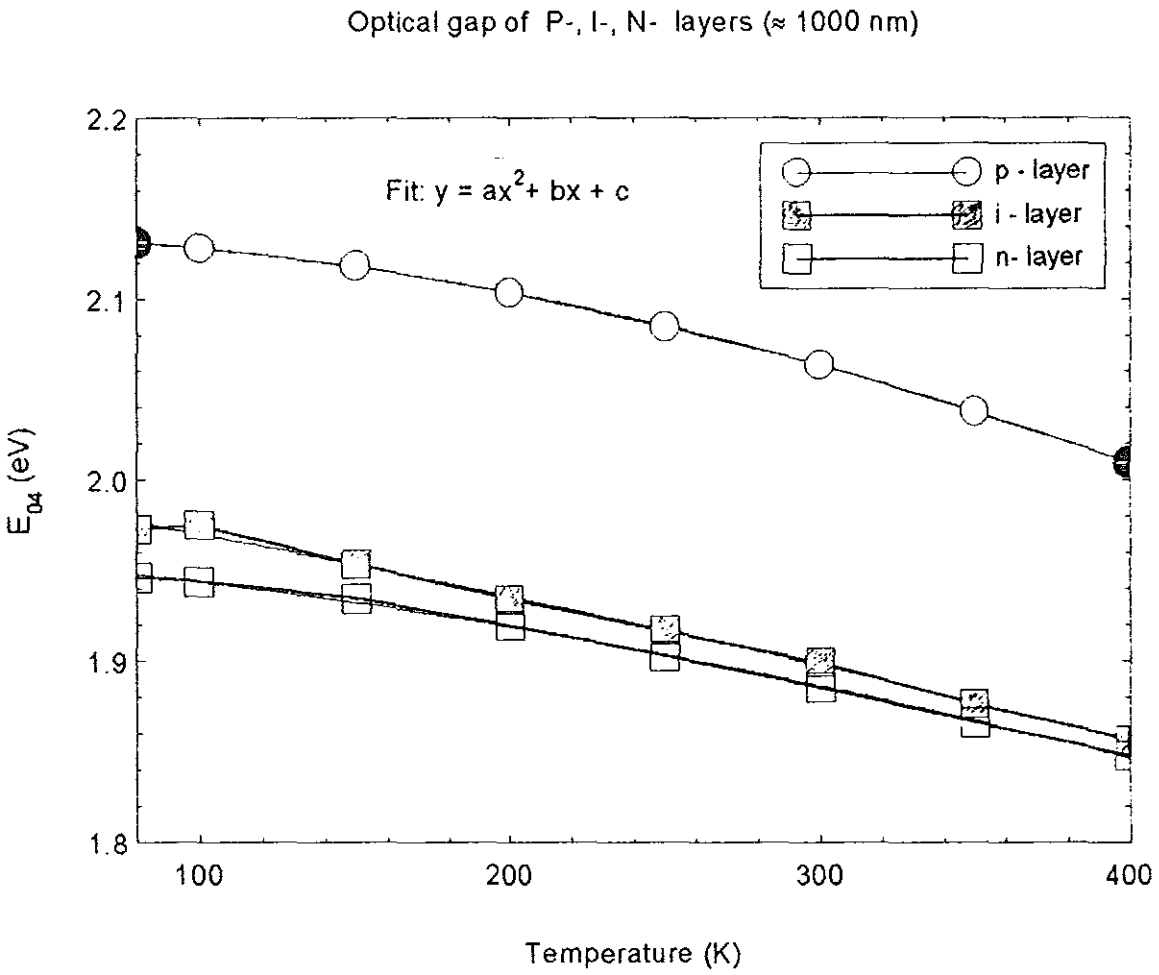

Figure 6.5 E_{04} as a function of temperature of p - , i - , and n - layers of a-Si:H films. E_{04} decreases when temperature increases.

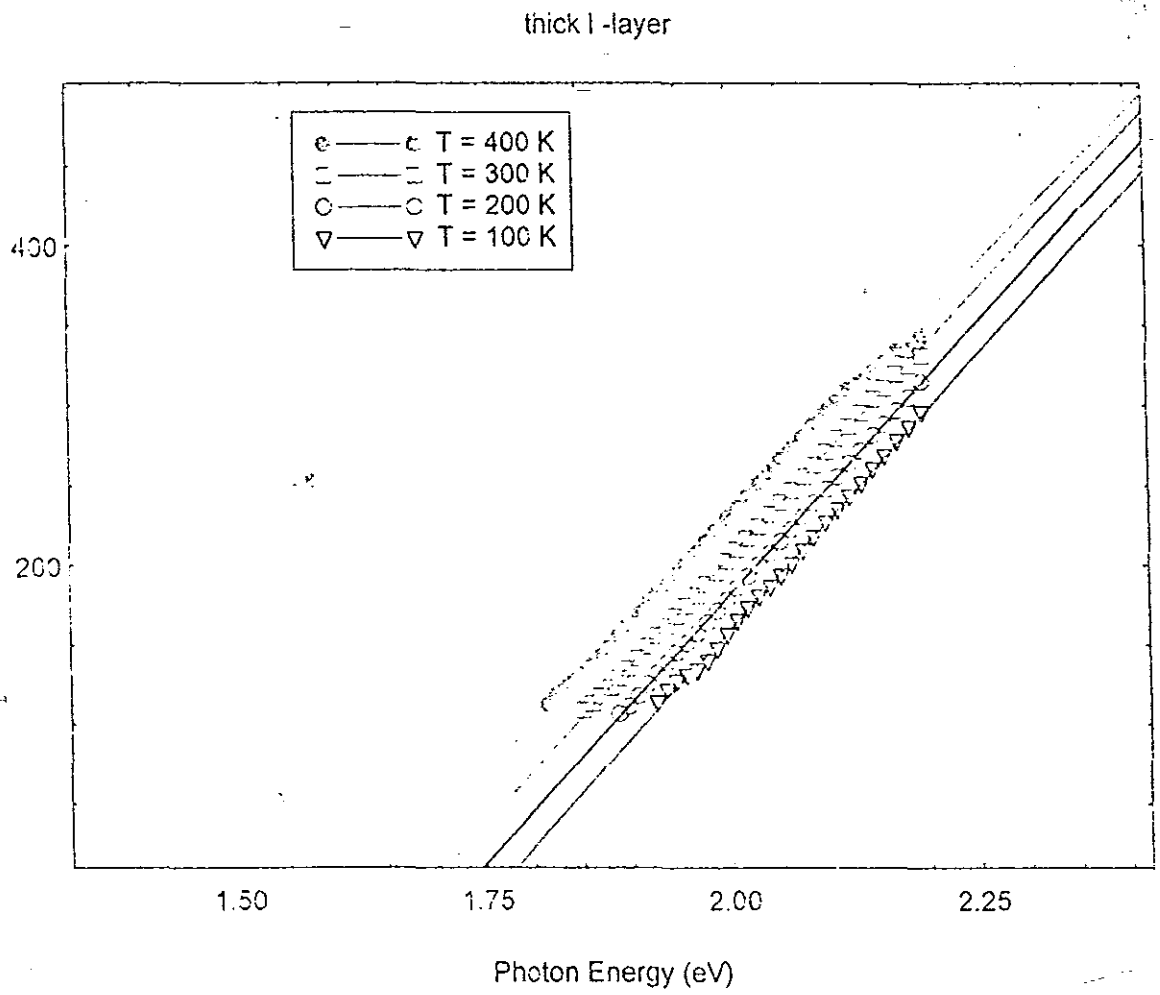

Figure 6.6 Tauc's plot at different temperatures of measurement.As temperature increases the Tauc's curve shifts towards lower energy.

Conclusion

The optical absorption coefficients measured at 400 K were about 20 % larger than those measured at room tempreture. Figure 6.6 shows the plot of $(\alpha E_{ph})^{1/2}$ vs E_{ph} . An excellent linearity was obtained. The optical band gaps were determined from the extrapolations of the plot of $(\alpha E)^{1/2}$ vs E . The optical band gaps decreased non - linearly with increasing operating temperature. This is in agreement with the Varshni's suggestion as the Debye temperature of c-Si is about 645 K [44] (if we assume the same order of magnitude for a- Si).The empirical relation given by Varshni states that the optical energy gap of semiconductors decreases non-linearly with increaseing temperature for the range of temperature less than deposition temperature of the film . The slope parameter A was about 633 $eV^{-1/2}cm^{-1/2}$ in our experiments . This is in good agreement with previous data [42]. It is known that short - circuit currents and open circuit voltages are directly related to the optical absorption coefficients and optical band gaps, respectively [3] . Therefore, short - circuit current increases with increase in temperature and the open circuit voltage decreases with increasing temperature. But obviously the carrier generation increases with increases in temperature due to increase in absorption .This fact could be of advantage for performance of solar cells if the photogenerated charge carriers could somehow be collected before the recombination occurs. Therefore, this result indicates that device remodeling is required for p-i-n type solar cells.

References

[1] United Solar System Corp. (UNI-SOLAR),"Announcement", Dr.Subhendu Guha, Tel . (313) 362 - 4170 , Fax 810\ 362 - 4442 ,(1993) USA.

[2] Physics Today, Sept.1993

[3] Wieder Sol. "An Introduction to Solar Energy for scientists and Engineers", John Wiley & Sons,1982

[4] Th.Eickhoff, C.Ulrichs, H.stiebig, W.Gruenen, W.reetz, and H.Wagner, 1st WCPEC HAWAII pp.622-625,1994

[5] Diego Fisher, These Prewsentee a la faculte des sciences pour obtenir de titre docteur es sciences Neuchtel, novembre 1994

[6] Arun Madan, Melvin P. Shaw, "The Physcs and Applications of Amorphous Semiconductors", Academic Press, Inc. P.176 (1988)

[7] J.M Berger, F. de Chelle, J. P Ferraton, A. Donnadieu, J. Beichler and G. Weiser, Solar Energy Materials 9, 301 - 309, North - Holland, 1983.

[8] Karoline Winz, "Messung und Interpretation Lateral Inhomogener Photostroeme in Duennerschichtsolarcellen aus amorphous Silicium, Diplomarbeit in Physik, Vorgelet der Mathematisch-Naturwissenschaftlichen fakultaet der Rheinsch-Westfaelichen Technischen Hochschule Aachen, im Oktober 1993

[9] M.L Theye, in Amorphous and Liquid Semiconductors, edited by J. Stuke and W. Brenig Taylor and Francis, London, p. 479,1974

[10] Bassani & Pastori Parravinci, "Electronic States and Optical Transitions in Solids" pp. 149-176, Academic Press

[11] S . Adachi, Phys.Rev. B 43, 12 316-12320 (1991)

[12] Czubatyj, W., Shur, M, Ng, K. and Madan, A. Proc. 14th IEEE Photovoltaic conference, San Diego, p.1214 (1980), IEEE, Newyork.

[13] M . Fried, Phys.Rev. B 49, 5699 (1994)

[14] M . L . Theye Physica Scripta Vol. T29 157-161 (1989)

[15] J . Tauc, R . Grigrorovici, and a . Vancu, Phys .Status Solidi 15, 627 (1966)

[16] Tatsuo Shimizu, Optoelectronics - Device and Technologies Vol.9, No.3, pp 277-298, Sept.1994

[17] David Adler," Chemistry and Physics of Covalent Amorphous Semiconductors", Department of Electrical Engineering and Computer Science ,Massachusetts Institute of Technology Cambridge, Massachusetts 02139, p.49 (1983)

18] Cohen, M . H., Fritzsche, H . and Ovshinsky, S. R (1969), Phys . Rev .22, 1065

[19] H .Fritzsche, Department of Physics and The James Franck Institute, University of Chicago, Chicago, Illinois 606 37 (1980)

[20] Adler, D .(1984) in " Semiconductors and Semimetals" (J . I . Pankove, ed), Vol.21, Part A ., Chapter 14, Academic press, Newyork.

[21] David Adler, Brain B . Schwartz and Martin C . Steele, " Physical Properties of Amorphous Materials" Institute for Amorphous Studies Series, 1995 pp 313-333

[22] Crandall, R . S, Williams, R ., and Tompkins, B.E (1979), J.App.Phys.50, 5506 (1979)

[23] A. R. Forouhi, I. Boomer, Phys. Rev. B 34, 7018-7026 (1986)

[24] C . D . Cody, " Semiconductors and Semimetals ", 21 part B, J . I . Pankove ed., chapter 2, p . 11, Academic Press, Newyork 1984

[25] Y . P . Varshni, Physica 34, 149-154 (1967)

[26] Moeglich, R . and Rompe, R . Z . bPhys. 119 472 (1942)

[27] Bardeen, J . and Shockley, W . , Phys .Rev .80 72 (1950)

[28] Fan, H. Y .Phys. Rev . 78 808 (1950)

[29] Fan, H .Y , Phys. Rev . 82 900 (1951)

[30] Muto T. and Yama, S . Prog. Theor. Phys. 5 833 (1950)

[31] Antoncik, E . Czech . J . Phys. 5 499 (1955)

[32] Vasileff, H . D . Phys . Rev. 105 441(1957)

[33] Adams, E . X ., Phys . Rev .167 671 (1957)

[34] E . Heaht and A .Zajac, Optics, Addison Wisley Pub.Comp., Newyork, (1987)

[35] K . L . Chopra, Thin Film Phenomena , Mc Graw - Hill Book Comp.Newyork. pp 723-793 (1969).

[36] Greenaway and Harbeke, Vol.1 " Optical properties and Band Structure of semiconductors" , Pergamon press p. 23 (1968)

[37] Cody,C .D., Wronski, C. R. , Abeles, B ., Stephens, R .B .,Brooks, B. Solar Cells 2,227 (1980).

[38] Klazes, R. H ., Van den Broek, M. H. L. M., Mezemer, J., and Radelarr, Phil. Mag. B45, 377 (1982)

[39] O. S Heavens, in " Thin Film Physics", Methuen & Co. Ltd. P. 63 (1970).

[40] Y. Hishikawa, S. Okamoto, K. Wakisaka, N. Nakamura, S. Tsada, S. Nakano, M. Ohnishi, and Y. Kawano., Ninth E.C. Photovoltaic Solar Energy Conference Freiburg (1989).

[41] Amensisa Abdi, Thesis, AAU, Optical Characterization of Thin Films for Solar Cell use (1994).

[42] Jin Seok Park and Min Koo Han, J. Appl. Phys. 65 (11), 1 June 1989

[43] G.weiser and H.Mell; Journal of Non-crystalline Solids 114, 298-300 (1989)

[44] N. M . Ravindra and V. K. Srivastava; J. Phys. Chem. Solids Vol. 40 pp.91-793

[45] H. Overhof P. Thomas," Electronic Transport in Hydrogenated Amorphous Semiconductors", Springer - Verlag , Berlin Heidelberg, P. 135 (1989).

[46] Arun Madan, Melvin P. Shaw, " The Physics and Applications of Amorphous Semiconductors", Academic Press, Inc. P. 325 (1988).